

Microstructural evolution and creep mechanism of a directionally solidified superalloy DZ125 under thermal cycling creep

Wenrui An¹, Satoshi Utada^{2,3}, Stoichko Antonov⁴, Song Lu¹, Silang He¹, Fan Lu¹, Weiwei Zheng¹, Longfei Li¹, Jonathan Cormier², Qiang Feng^{1*}

¹ Beijing Advanced Innovation Center for Materials Genome Engineering, State Key Laboratory for Advanced Metals and Materials, University of Science and Technology Beijing, Beijing, 100083, China

² Institut Pprime, CNRS – ENSMA – Université de Poitiers, UPR CNRS 3346, Physics and Mechanics of Materials Department, ISAE-ENSMA – Téléport 2, 1 avenue Clément Ader, BP 40109, 86961 Futuroscope Chasseneuil Cedex, France

³ Department of Materials, University of Oxford, Parks Road, Oxford, OX1 3PH, United Kingdom

⁴ Department of Microstructure Physics and Alloy Design, Max-Planck-Institut für Eisenforschung GmbH, Düsseldorf 40237, Germany

Abstract:

In this study, thermal cycling creep tests under (950 °C/15 min+1100 °C/1 min)-100 MPa were performed to simulate the overheating service condition of a directionally solidified superalloy DZ125. The microstructural evolution and creep mechanism at each creep stage were revealed by systematic microstructure characterization after the interrupted creep tests. The results indicated that DZ125 superalloy exhibited three creep stages: the decelerating stage, the slow accelerating stage and the rapid accelerating stage. During creep, the un-recovered γ' volume fraction at the lower temperature stages and the deterioration of grain boundary caused by the overheating stages were harmful to the creep resistance. During the decelerating stage, a few dislocations moved on the γ matrix. The rafted γ' microstructure and dislocation networks formed near the minimum creep rate. Simultaneously, some dislocations sheared the γ' phase as well. During the slow accelerating stage, the rafted γ' microstructure and dislocation networks could prevent dislocations from moving. However, the dislocations shearing the γ' phase, facilitated by the overheating and thermal cycling process, was conducive to creep deformation. During the rapid accelerating stage, more dislocations shearing the γ' phase, severe γ' phase degradation and increasing PFZs (precipitate free zones) along the grain boundary accelerated the creep deformation. The coupled effect of overheating and thermal cycling damage accelerated the deformation during the thermal cycling creep.

Keywords:

Directionally solidified superalloy DZ125, thermal cycling creep, microstructural evolution, deformation mechanism.

1. Introduction

Ni-based superalloys are widely utilized in hot-section components of advanced aero-engines, e.g., turbine blades, due to their excellent performance at high temperature[1]. During service, turbine blades are subjected to fluctuating temperatures as well as non-constant loads. Therefore, overheating becomes an inevitable issue which can lead to serious microstructural degradation or even result in premature failure of turbine blades. For instance, failure analysis examination of overheated blades during service operations demonstrates the dissolution of the strengthening phase and even incipient melting of these components due to overheating[2]. To better address such conditions, non-isothermal testing has been established to estimate the overheating effect by building the relationship between the overheating condition, microstructural degradation and mechanical property in some Ni-based single crystal (SX) superalloys[3-9].

Until now, two typical types of non-isothermal creep tests have been conducted: Type I, creep test with a single overheating event; Type II, creep test with periodic overheating events, i.e., thermal cycling creep. Type I focus on the overheating effect at different creep stages, in order to recognize the effects of overheating time, duration and temperature on the creep properties[3, 10]. Type II (thermal cycling creep) deals with investigating the effects of overheating frequency and temperature on the creep properties[7, 9, 11]. The results clearly show that the non-isothermal or thermal cycling creep life is drastically reduced compared with the isothermal creep life [9, 11]. The inferior creep properties were mainly ascribed to the microstructural degradation caused by the overheating events, such as the dissolution of the γ' phase and the unfavorable substructural evolutions[7, 11]. The microstructure varies at different stages of a thermal cycle; for example, the γ' phase dissolves at the overheating stage and recovers at the lower temperature stage[5, 12, 13]. Importantly, early dislocation shearing of the γ' phase promoted by thermal cycling leads to the earlier minimum creep rate[7]. In recent years, some researches on the thermal cycling creep of conventional cast (CC) superalloys have also been published[14, 15]. The results indicate that the grain boundaries and carbides, which are typical features of CC superalloys, were prone to crack initiation during the thermal cycling creep[14, 15]. However, there was still no systematic study on the

microstructural evolution and deformation mechanism at different thermal cycling creep stages.

Directionally solidified (DS) superalloys eliminate transverse grain boundaries and greatly improve the high-temperature mechanical properties compared with those of CC superalloys[16, 17]. Meanwhile, DS superalloys comprise of more carbides and γ/γ' eutectics pools compared to SX superalloys. These microstructural features and the columnar grain boundaries are typically the weak zones during the creep of DS superalloys[18-21]. In our previous research on the thermal cycling creep, DS superalloy DZ125 exhibited similar three creep stages and considerably shortened creep life compared to the isothermal creep[22, 23]. The plastic strain mainly accumulated during the overheating stages of thermal cycling creep[22]. Moreover, each thermal cycle promoted dislocations to shear the γ' phase, leading to the earlier macroscopical minimum creep rate[22]. In addition, the grain boundaries, carbides and γ/γ' eutectics pools were also prone to crack initiation[22, 23]. As turbine blades may undergo overheating at service, it is critical to investigate the creep mechanisms of these superalloys at various stages during the thermal cycling creep.

In this study, the interrupted tests were performed at different accumulated plastic strain and thermal cycle locations during the thermal cycling creep of DZ125 superalloy, and the systematic characterization of microstructural evolution and dislocation configurations were conducted within grains and grain boundaries. The deformation mechanism of DZ125 superalloy at different stages of thermal cycling creep were revealed, and the difference of thermal cycling creep mechanism in SX, DS and CC superalloys were discussed. The results are significant for an in-depth understanding of overheating service damage and provide a reference for the maintenance of DS superalloy blades to enable service safety.

2. Materials and methods

The DS superalloy DZ125 used in the present study has a nominal chemical composition (wt.%) as 10.0Co, 8.9Cr, 7.0W, 5.2Al, 2.0Mo, 3.8Ta, 1.5Hf, 0.9Ti, 0.1C, 0.015B and balanced by Ni, and was directionally solidified into $\Phi 15 \times 170$ mm cylindrical bars along the [001] orientation by the high-rate solidification (HRS) process at the Beijing Institute of Aeronautical Materials (BIAM). All the bars were subjected to the standard heat treatment of 1180 °C/2 h +1230 °C/3 h with air cooling (AC) + 1100 °C/4 h (AC) + 870 °C/20 h (AC).

In order to ensure the uniformity of the microstructure and comparability of the creep properties, all creep specimens with 4 mm in diameter and 14 mm in gauge length were machined from the homogeneous crystal zone of the same batch of DS bars. The EBSD results showed that each specimen consists of several columnar crystals with orientations within 5°

from $\langle 001 \rangle$. The thermal cycling creep tests were conducted in a Lever Arm Setra SF 2400 creep rig equipped with a radiant heating furnace, which was capable of fast heating and cooling during the creep test; more details can be found in Ref.[7]. The thermal cycling creep tests were conducted at cycle conditions of (950 °C/15 min-1100 °C/1 min)/100 MPa, i.e., the creep stress was constant at 100 MPa, and the temperature was changed cyclically. Figure 1 depicts the temperature profile of the thermal cycling creep test. Each cycle consisted of 15 minutes at the lower temperature of 950 °C and 1 minute at the overheating temperature of 1100 °C, and the heating and cooling rates were 100 °C/min and 600 °C/min, respectively. Interrupted thermal cycling creep tests were performed at different thermal cycle locations under specific plastic strain to investigate the differences in the temperature-affected microstructures. The interrupted locations of the thermal cycle are selected at: (1) the end of the 950 °C stage (just before heating), (2) the end of the 1100 °C stage (just before cooling) and (3) 1 min of the 950 °C stage (after the temperature cooled back to the lower temperature); these are referred to as 1#, 2# and 3#, respectively, as shown in Figure 1. Here, the comparison of the microstructure between the 1# and 2# specimens should reveal the microstructural evolution during the heating process and holding at 1100 °C stage. The comparison of the microstructure between 2# and 3# specimens should reveal the microstructural evolution during the cooling process. It is worthy to note the microstructure of 1# and 1' in the subsequent cycle was assumed to be nearly the same. Thus, the microstructure in 1' is neglected for simplicity in this study. The microstructural evolution during the 950 °C stage could be revealed by comparing the difference between 3# and 1# specimens instead of 1'. All the specimens are named as “N_{plastic strain}—thermal cycle location” for a brief description, e.g., the “N_{0.5}-2#” referred to the specimen interrupted at the 2# location of a thermal cycle with 0.5% plastic strain. Table 1 lists the creep condition and the name of all the specimens.

Metallographic specimens were prepared on the cross section (perpendicular to the loading stress) and longitudinal section (parallel to the loading stress) of the interrupted creep specimens. After standard grinding and polishing, the specimens underwent electrolytic etching in a solution containing 12 vol.% phosphoric, 40 vol.% nitric and 48 vol.% sulfuric acids at 3 V for about 3 s. The microstructure characterization was conducted by a ZEISS SUPRA 55 field-emission scanning electron microscope (FE-SEM). The γ' volume fraction in the dendrite core region on the cross section was quantified by the manual point count method according to the ASTM E562 Standard[24]. The γ channel width on the longitudinal section and the γ' rafting degree (Ω)[25] were measured by MATLAB and Photoshop software. For each condition, 4 to 5 images were used for measurements to obtain statistically significant results. The linear

density of a typical microstructure along the grain boundary was defined by the l_c/l ratio, where l_c was the length of the grain boundary that was filled with specific microstructure and l is the length of whole grain boundary[26]. Grain boundaries with a total length of 2 mm were continuously scanned along the longitudinal section by SEM and the statistics were conducted by ImageProPlus software. An Oxford Symmetry electron backscatter diffraction (EBSD) probe operated on a JSM-7900 F Plus SEM was used to identify the number of grains on the cross section of each interrupted creep specimen. The EBSD specimens were prepared by the mentioned standard grinding, polishing and extra 5 h stress-relieve polishing.

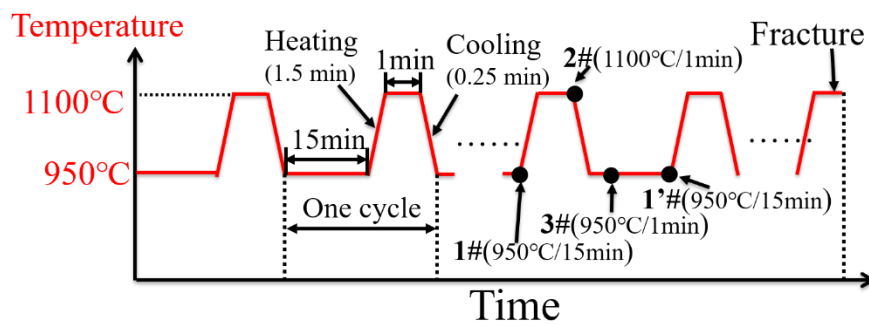


Figure 1—The temperature profile of the thermal cycling creep testing and the interrupted test locations

Table 1— Specimen name, creep time, plastic strain and number of grains in DZ125 superalloy after interrupted at different strains and thermal cycle locations during the thermal cycling creep under (950 °C/15 min-1100 °C/1 min)/100 MPa

Specimen name	Creep condition		Plastic strain/%	Time/h	Number of grains
N _{0.1} -1#	Interrupted creep tests	15 min at 950 °C	0.24	1.77	9
N _{0.1} -2#	with 6 th cycle (~ 0.1% strain)	End of 1100 °C	0.07	1.51	14
N _{0.1} -3#		1 min at 950 °C	0.14	1.54	28
N _{0.5} -2#	Interrupted creep tests with 0.5% plastic strain	End of 1100 °C	0.50	12.37	14
N _{1.0} -1#	Interrupted creep tests with 1% plastic strain	15 min at 950 °C	1.00	10.84	17
N _{1.0} -2#		End of 1100 °C	1.00	23.72	8
N _{1.0} -3#		1 min at 950 °C	1.00	20.10	7
N _{5.0} -1#	Interrupted creep tests with 5% plastic strain	15 min at 950 °C	5.00	67.10	7
N _{5.0} -2#		End of 1100 °C	5.00	42.44	13
N _{5.0} -3#*		1 min at 950 °C	~5.00	42.55	26

Note: * The extensometer failed during the test, so the interruption was determined by the test time.

The dislocation configurations were observed using a transmission electron microscope

(TEM)—FEI TECNAI G2 F30. Thin foils for TEM observations were prepared by the twin-jet electro-polishing technique in a solution containing 4 vol.% CH₃COOH, 8 vol.% HClO₄ and 88 vol.% C₂H₅OH at 50 V and -35 °C. 10 TEM images were taken under the two-beam condition to statistically measure the average dislocation network spacing.

3. Results

3.1. Creep properties

Figure 2(a) depicts the individual accumulated plastic strain vs. time curves of DZ125 superalloy during the whole thermal cycling creep process at (950 °C/15 min-1100 °C/1 min)/100 MPa as well as in the 950 °C stages and overheating stages of the thermal cycle, respectively. The overheating stage includes the 1100 °C stage and heating/cooling process. Details about the data processing can be found in Ref.[22]. The thermal cycling creep life is 96.2 h with a plastic strain of ~29% at failure, as presented by the red line. The individual accumulated plastic strain in the overheating stages (purple line) was close to that of the total creep strain, even slightly higher after ~60 h. At the same time, the accumulated plastic strain in the 950 °C stages (green line) was minimal.

Figure 2(b) depicts the plastic strain rate vs. time curve of DZ125 superalloy derived from the red line in Figure 2(a). The whole thermal cycling creep process was divided into three stages based on the variation of strain rate: the decelerating stage, the slow accelerating stage and the rapid accelerating stage. During the decelerating stage, the strain rate decreased rapidly, reaching the minimum value of $\sim 1.18 \times 10^{-7} \text{ s}^{-1}$ at 11.7 h and 0.36% plastic strain as marked by a star. At this point, the slow accelerating stage initiated. Finally, a transition point of the strain rate was detected at ~67 h and ~4.6% plastic strain. The strain rate increased rapidly until the fracture as labeled by the rapid accelerating stage in Figure 2(b). The values for creep time, plastic strain and strain rate of the three creep stages are listed in Table 2. Interrupted creep tests were further conducted to different plastic strains such as 0.1% at the decelerating stage, 0.5% near the minimum creep rate or the beginning of the slow accelerating stage, 1.0% at the slow accelerating stage and 5.0% at the rapid accelerating stage to study the thermal cycling creep mechanisms, as marked by the black circles in Figure 2(b).

Table 1 lists all the specimen names, creep time, plastic strain and the number of grains on the cross section after the interrupted thermal cycling creep tests. The creep time of the specimens exhibited noticeable scatter under the same plastic strain. The data in Table 1 indicates that the creep time under 0.1% plastic strain was not affected by the number of grains,

but under a plastic strain of 1% and 5%, generally, the lower the number of grains, the longer the creep time. That is, there was a simple negative correlation between the number of grains and the creep properties.

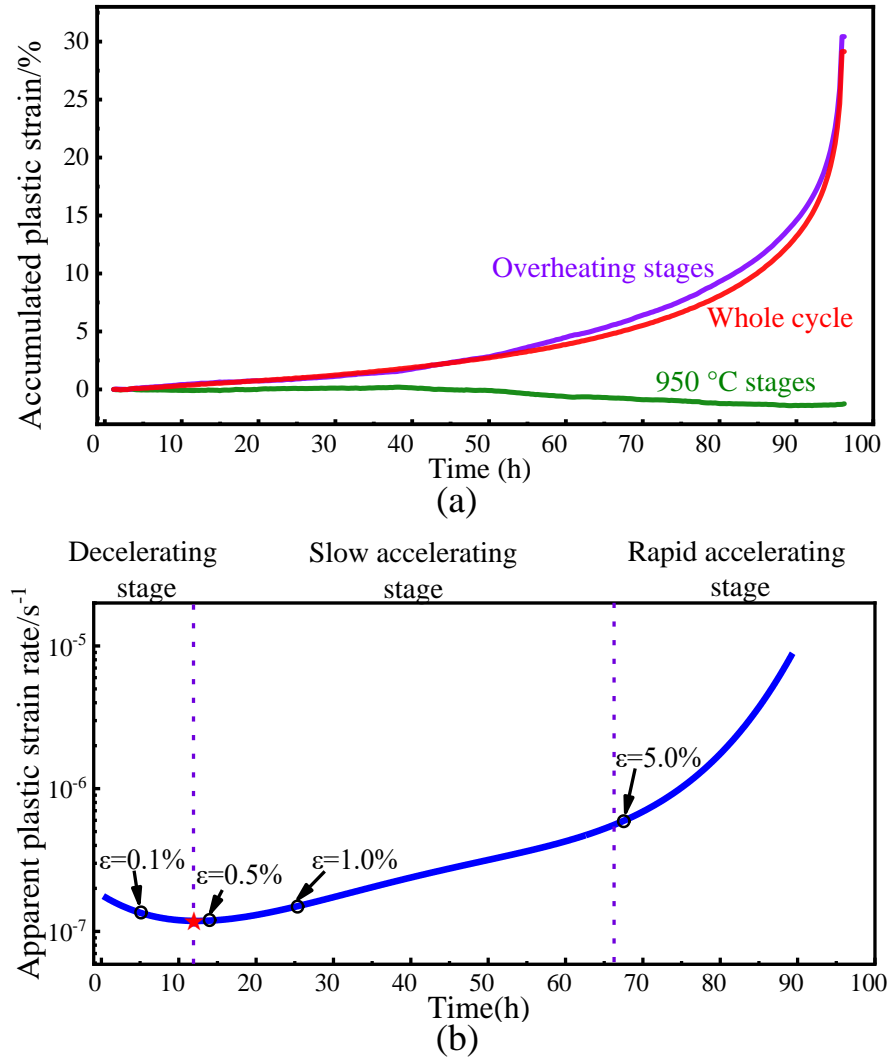


Figure 2—Creep curves of DZ125 superalloy under the (950 °C/15 min-1100 °C/1 min)/100 MPa thermal cycling creep: (a) accumulated plastic strain vs. time curve during different stages of the thermal cycle, (b) apparent plastic strain rate vs. time curve and the interrupted locations.

Table 2—Creep time, plastic strain and strain rate at different stages of DZ125 superalloy during the thermal cycling creep under (950 °C/15 min-1100 °C/1 min)/100 MPa

Creep stage	Time/h	Plastic strain/%	Strain rate/ $10^{-7} s^{-1}$
Decelerating stage	0~11.7	0~0.36	1.77~1.18
Slow accelerating stage	11.7~67.0	0.36~4.60	1.18~5.81
Rapid accelerating stage	67.0~96.2	4.60~29.14	5.81~88.92

3.2. Microstructural evolution during the thermal cycling creep

In this study, microstructural observation and characterization were conducted for every interrupted thermal cycling creep specimen to analyze the microstructural and substructural evolution.

(1) Microstructural evolution in the primary dendritic core area

Figure 3(a1~a3) displays the typical γ/γ' microstructure in the primary dendrite core on the cross section of DZ125 superalloy after the interrupted thermal cycling creep with 0.1% plastic strain during the decelerating stage. The primary γ' phase in N_{0.1-1#}, N_{0.1-2#} and N_{0.1-3#} specimens has dissolved significantly compared with the as-received state[22] (γ' phase refers to the primary γ' phase in the following unless otherwise noted). Generally, the majority of γ' phase remained nearly cuboidal with round corners, while some γ' phase was an agglomerate of smaller size. The γ' phase did not coarsen but connected slightly in some areas (the black arrows in Figure 3(a1~a3)). Concurrently, some fine secondary γ' phase precipitated in the γ matrix, which was more pronounced in N_{0.1-1#} and N_{0.1-3#} specimens rather than N_{0.1-2#} specimen. It is indicated that secondary γ' phase precipitated during the cooling stage of the thermal cycle and dissolved during the heating and 1100 °C stages of the thermal cycle. The γ' volume fraction in N_{0.1-1#}, N_{0.1-2#} and N_{0.1-3#} specimens was 48.9%, 46.3% and 48.2%, respectively, which were all significantly lower than that of the as-received state (67.6%, Ref.[22]). Their average size of the γ' phase were 0.54 μm , 0.45 μm and 0.54 μm , respectively. Figure 3(b1~b3) demonstrates the typical microstructure in the dendrite core on the longitudinal section of N_{0.1-1#}, N_{0.1-2#} and N_{0.1-3#} specimens. The γ' phase on the longitudinal section was only slightly elongated in the direction perpendicular to the stress axis without the obvious rafting (the black arrows in Figure 3(b1~b3)). As a whole, Figure 3 demonstrates that the γ' phase was similar at different thermal cycle locations under 0.1% plastic strain during the decelerating stage, but did undergo a dramatic decrease in γ' volume fraction and a slight change in morphology compared to the as-received state.

Figure 4 shows the typical γ/γ' microstructure in the primary dendrite core on the cross section and longitudinal section of N_{0.5-2#} specimen, which was interrupted near the minimum creep rate or the beginning of the slow accelerating stage. Figure 4(a) demonstrates that the γ' phase on the cross section coarsened obviously. The majority of γ' phase connected and agglomerated with rounded edges. Here, some γ phase was embedded as a result of γ' phase coalescence in the form of independent islands, as marked by the black arrows in Figure 4(a). The γ' volume fraction of N_{0.5-2#} specimen was 48.9%, which was the same as that at 0.1%

plastic strain. Figure 4(b) demonstrates the typical microstructure in the dendrite core on the longitudinal section of N_{0.5}-2# specimen. An early stage of rafted γ' microstructure was observed as most of γ' precipitates coarsened and connected along the direction perpendicular to the stress axis, and only a few γ' precipitates connected longitudinally (black arrows in Figure 4(b)). The rafting degree was 0.35, and the γ channel width on the longitudinal section was 466 nm. Figure 4 indicates that γ' morphology degraded significantly near the minimum creep rate.

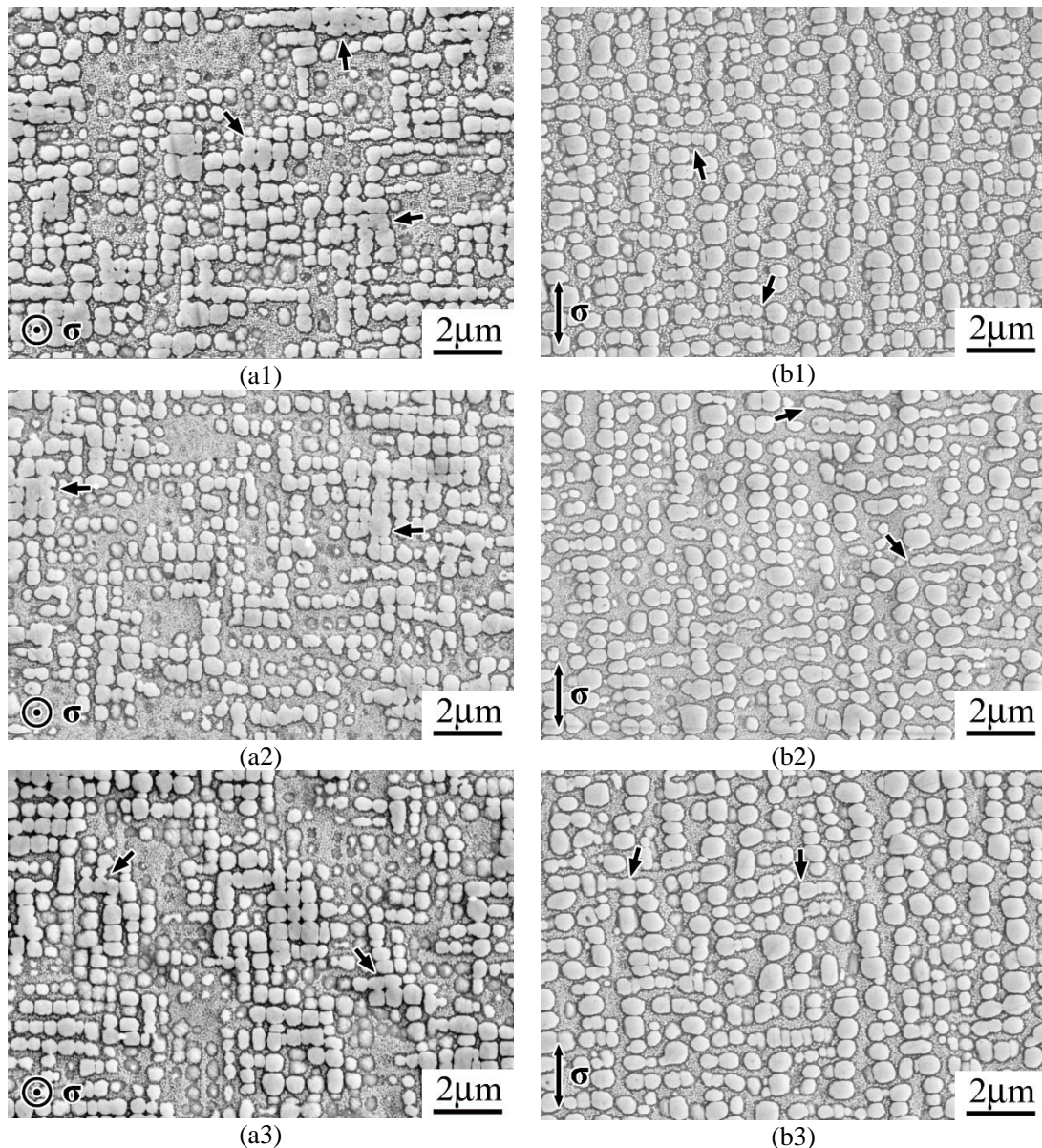
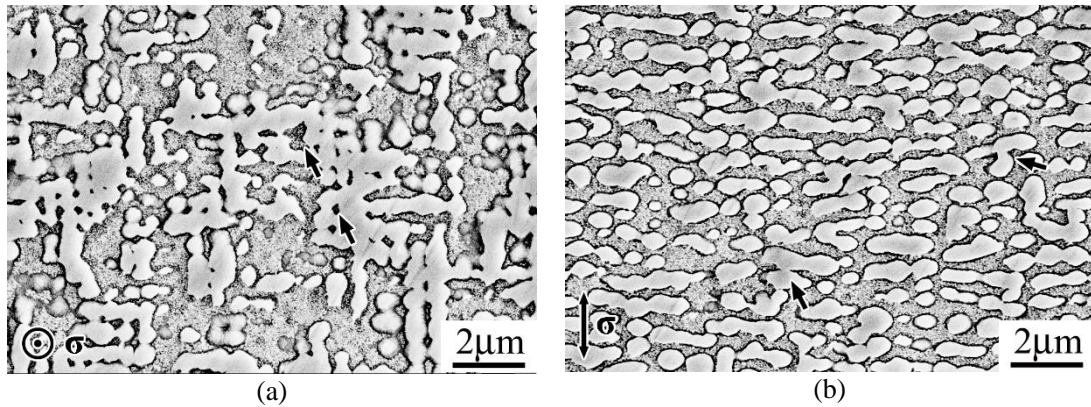


Figure 3—SEM images of γ/γ' microstructure in the primary dendrite core of DZ125 superalloy after the interrupted thermal cycling creep with 0.1% plastic strain on the (a) cross section and (b) longitudinal section of (1) N_{0.1}-1#, (2) N_{0.1}-2# and (3) N_{0.1}-3# specimens. The slightly connected γ' precipitates on the cross section and slightly elongated γ' precipitates on the

236 longitudinal section are marked by the black arrows in (a) and (b), respectively.



238 Figure 4—SEM images of γ/γ' microstructure in the primary dendrite core of $N_{0.5-2\#}$ specimen
on the (a) cross section and (b) longitudinal section. The γ islands surrounded by γ' precipitates
240 and longitudinally connected γ' precipitates are marked by the black arrows in (a) and (b),
respectively.

242 Figure 5(a1~a3) depicts the typical γ/γ' microstructure in the primary dendrite core on the
cross section of DZ125 superalloy after the interrupted thermal cycling creep with 1.0% plastic
244 strain during the slow accelerating stage. The majority of γ' precipitates in $N_{1.0-1\#}$, $N_{1.0-2\#}$ and
 $N_{1.0-3\#}$ specimens coalesced into the morphology with rounded edges. The minority of γ'
246 precipitates exhibited small size and rounded shape. Also, some γ phase was embedded by
coalesced γ' phase as independent islands. Among these three specimens, $N_{1.0-2\#}$ specimen
248 shows a more serious microstructural degradation in terms of a lower γ' volume fraction, more
coarsened γ' phase and less secondary γ' phase. The γ' volume fraction of $N_{1.0-1\#}$, $N_{1.0-2\#}$ and
250 $N_{1.0-3\#}$ specimens were 49.0%, 46.0% and 45.1%, respectively. Figure 5(b1~b3) demonstrates
the typical γ/γ' microstructure in the dendrite core on the longitudinal section of $N_{1.0-1\#}$, $N_{1.0-}$
252 $2\#$ and $N_{1.0-3\#}$ specimens. An N-type rafted γ' microstructure with relatively smooth interfaces
was formed and still a few γ' precipitates connected along the loading direction (black arrows
254 in Figure 5(b)). The rafting degree of $N_{1.0-1\#}$, $N_{1.0-2\#}$ and $N_{1.0-3\#}$ specimens were 0.29, 0.39
and 0.41, respectively. The γ channel width of $N_{1.0-2\#}$ specimen was wider than that of $N_{1.0-1\#}$
256 and $N_{1.0-3\#}$ specimens. Figure 5 indicates that the morphology of γ' phase degraded severely
at the 1100 °C stage of the thermal cycle. At the same time, the γ' phase degraded to a higher
258 extent with increasing the strain during the slow accelerating stage.

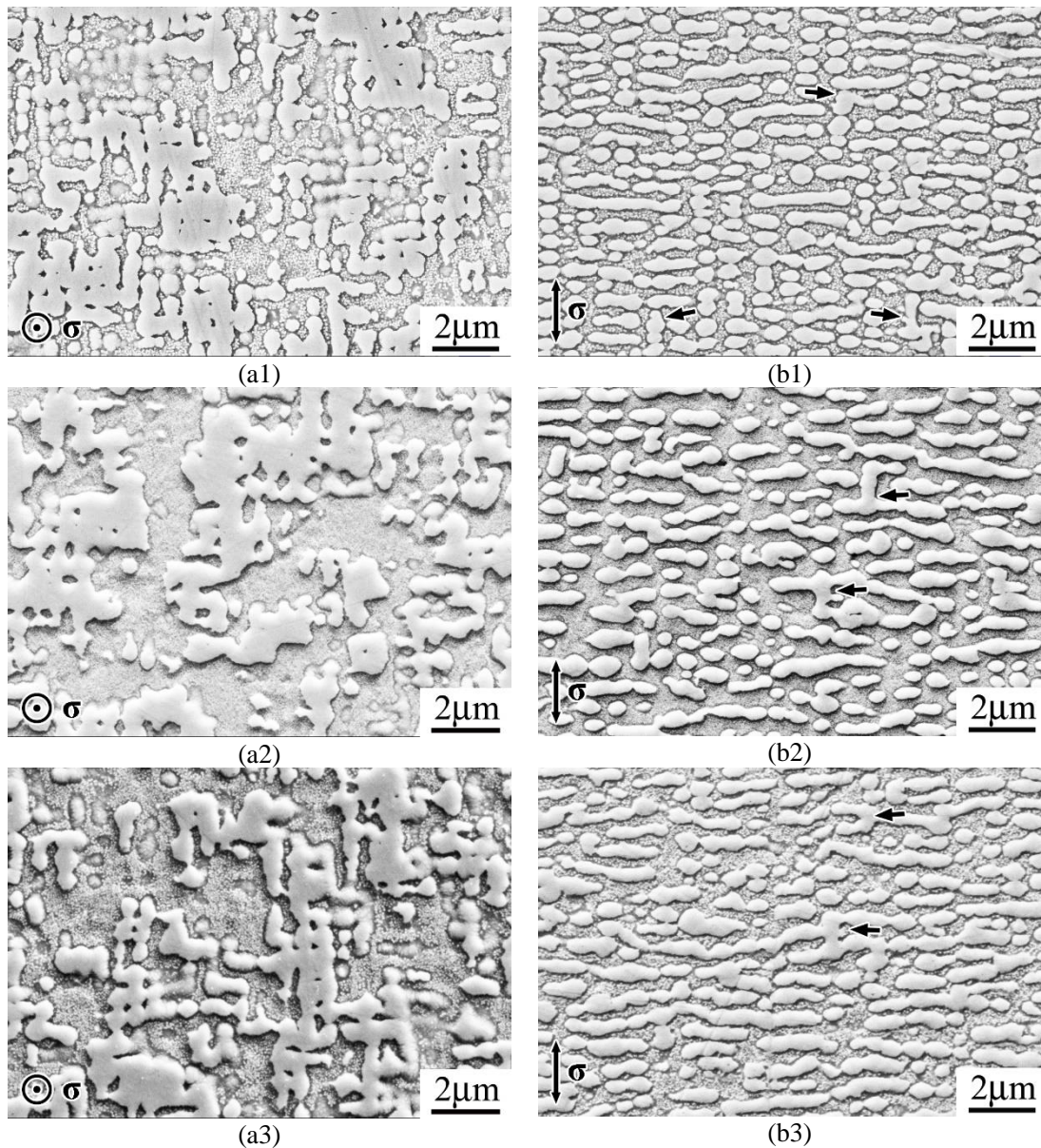
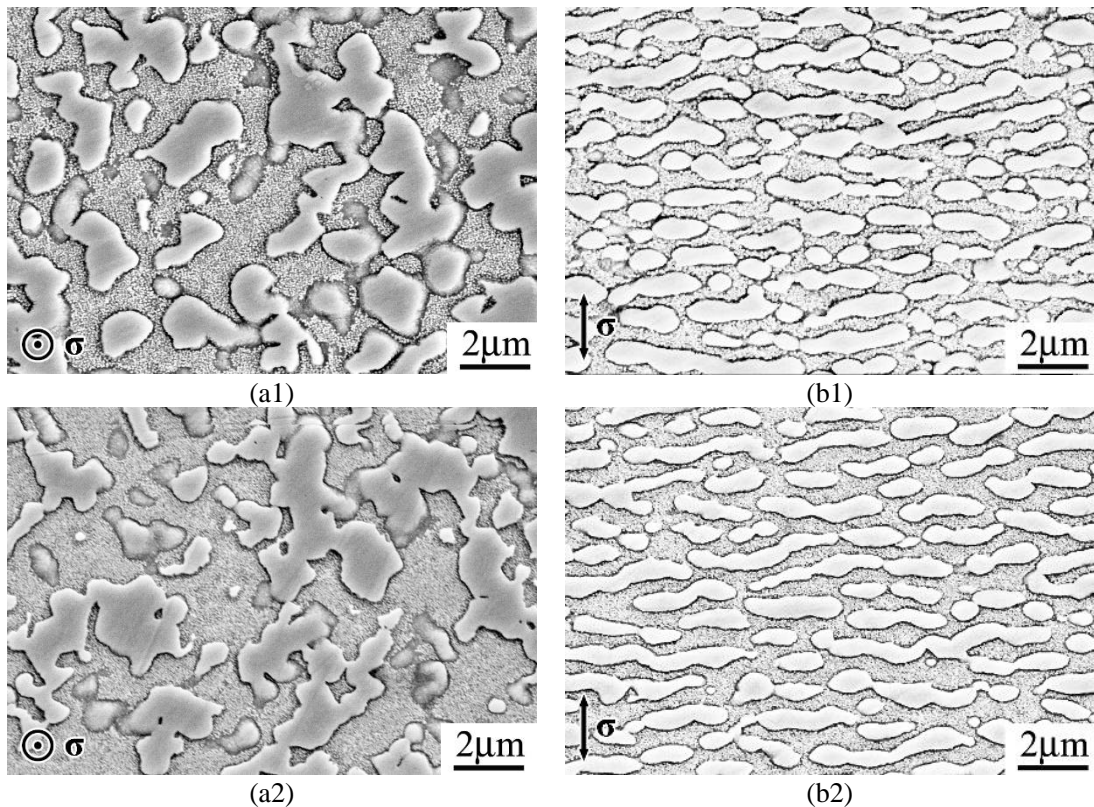


Figure 5—SEM images of γ/γ' microstructure in the primary dendrite core of DZ125 superalloy after the interrupted thermal cycling creep with 1.0% plastic creep strain on the (a) cross section and (b) longitudinal section of (1) N_{1.0}-1#, (2) N_{1.0}-2# and (3) N_{1.0}-3# specimens. The longitudinally connected γ' precipitates are marked by the black arrows in (b).

Figure 6(a1~a3) depicts the typical γ/γ' microstructure in the primary dendrite core on the cross section of DZ125 superalloy after the interrupted thermal cycling creep with 5.0% plastic strain during the rapid accelerating stage. The γ' morphology of N_{5.0}-1#, N_{5.0}-2# and N_{5.0}-3# specimens were similar, where it lost its original rectangular edges and coalesced more severely compared to the γ' phase under 1.0% plastic strain. The fine secondary γ' precipitates in the γ matrix of N_{5.0}-1# and N_{5.0}-3# specimens were more evident than those in N_{5.0}-2# specimen. Combining with Figure 3(a1~a3), it is evidently indicated that secondary γ' phase precipitated

during the cooling stage of the thermal cycle and dissolved during the heating and 1100 °C stages of the thermal cycle. The γ' volume fraction of N_{5.0}-1#, N_{5.0}-2# and N_{5.0}-3# specimens were 44.6%, 45.0% and 44.2%, respectively, which were slightly lower than those under 1.0% plastic strain. Figure 6(b1~b3) shows the typical microstructure in the dendrite core on the longitudinal section of N_{5.0}-1#, N_{5.0}-2# and N_{5.0}-3# specimens. A well-developed N-type rafted γ' microstructure was formed, which had smoother interfaces and wider γ channels than under 1.0% plastic strain. The rafting degree of N_{5.0}-1#, N_{5.0}-2# and N_{5.0}-3# specimens were 0.45, 0.46 and 0.41, respectively. The γ channel width of N_{5.0}-2# specimen was wider than these of N_{5.0}-1# and N_{5.0}-3# specimens. It is evident in Figure 6 that the morphology and volume fraction of γ' phase were similar at different thermal cycle locations under 5.0% plastic strain, except that the γ channels were wider at the 1100 °C stage. During the rapid accelerating stage, the γ' phase degraded more severely than that at the slow accelerating stage (1.0% plastic strain, Figure 5).



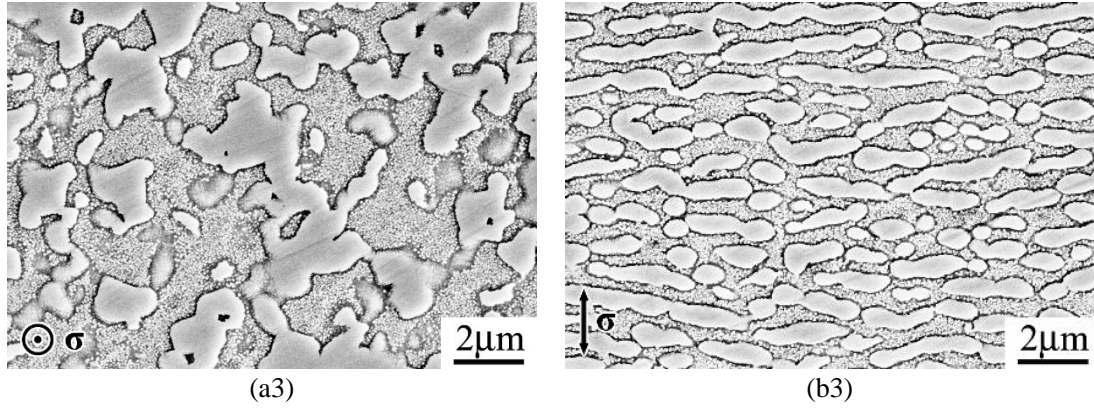


Figure 6—SEM images of γ/γ' microstructure in the dendrite core of DZ125 superalloy after the interrupted thermal cycling creep with 5.0% plastic creep strain on the (a) cross section and (b) longitudinal section of (1) N_{5.0}-1#, (2) N_{5.0}-2# and (3) N_{5.0}-3# specimens.

Table 3 summarizes the quantitative γ' volume fraction, rafting degree of γ' phase and width of γ channel in DZ125 superalloy under the interrupted thermal cycling creep conditions. In order to visually compare the microstructural evolution during the thermal cycling creep, the statistic parameters in Table 3 are plotted in Figure 7.

Table 3—Quantitative volume fraction of γ' phase, rafting degree of γ' phase, width of γ channel and average dislocation network spacing of DZ125 superalloy under the interrupted thermal cycling creep conditions

Specimen name	γ' volume fraction/%	Rafting degree, Ω	Width of γ channel/nm	Average dislocation network spacing/nm
As-received	67.6±3.1	N/A	N/A	N/A
N _{0.1} -1#	48.9±3.7	N/A	256±24	N/A
N _{0.1} -2#	46.3±1.5	N/A	278±57	N/A
N _{0.1} -3#	48.2±2.4	N/A	274±45	N/A
N _{0.5} -2#	48.9±4.2	0.35	466±27	95±11
N _{1.0} -1#	49.0±3.8	0.29	427±27	90±9
N _{1.0} -2#	46.0±4.0	0.39	480±10	98±12
N _{1.0} -3#	45.1±2.9	0.41	444±30	96±10
N _{5.0} -1#	44.6±2.6	0.45	626±76	75±11
N _{5.0} -2#	45.0±2.9	0.46	645±56	64±10
N _{5.0} -3#	44.2±1.4	0.41	621±70	68±8

(2) Microstructural evolution along the grain boundaries during creep

Compared to SX superalloys, DS superalloys contain more carbides and γ/γ' eutectic pools in the interdendritic region, in addition to grain boundaries. In this study, the interdendritic

region microstructure slightly changed after 5.0% plastic strain compared with the as-received state (images not shown here). Therefore, the following part will focus on the microstructure along the grain boundary.

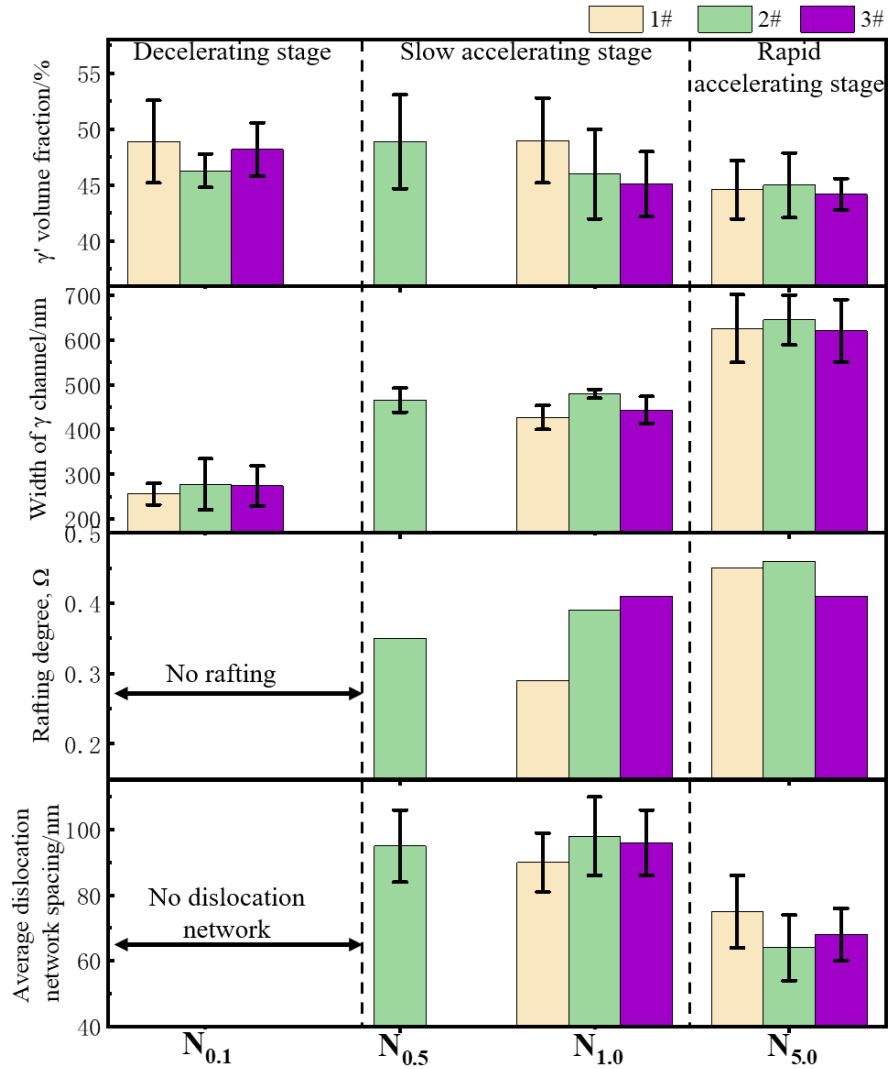
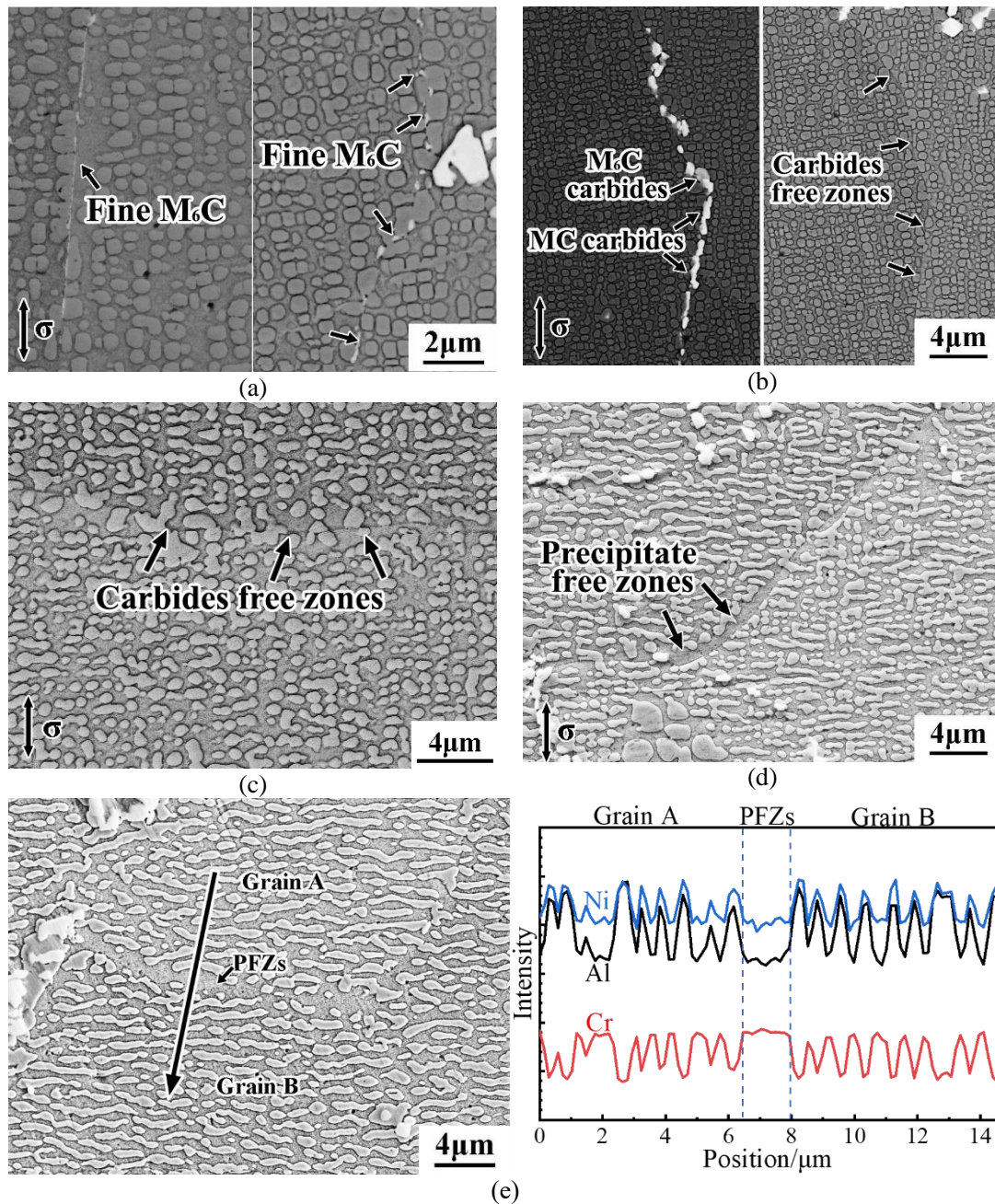


Figure 7 The γ' volume fraction, rafting degree of γ' phase, width of γ channel and average dislocation network spacing of DZ125 superalloy under the interrupted thermal cycling creep conditions

The previous study observed MC carbide chains and fine M_6C carbides along the grain boundaries in the as-receive state[22]. Figure 8 demonstrates the typical microstructure along the grain boundary of DZ125 superalloy after the interrupted thermal cycling creep with different plastic strains. In this study, the microstructure along the grain boundaries seems to be similar at different thermal cycle locations with the same plastic strain. Figure 8(a~b) depicts the microstructure along the grain boundary of $N_{0.1}$ -2# specimen. There were fine gray carbides

with the size of $\sim 0.1\ \mu\text{m}$ (Figure 8(a)) and carbide chains with the size of $0.5\sim 1\ \mu\text{m}$, which consisted of many light-gray contrast carbides and a few darker-gray carbides (Figure 8(b)). In reference to the SEM-EDS results and the previous research[27], the above dark-gray carbides are M_6C and the light-gray carbides are MC, as marked in Figure 8(a~b). Meanwhile, there are also some carbide free zones (CFZs) along the grain boundaries in $\text{N}_{0.1-2\#}$ specimen, where only the dispersed γ' phase was observed, as marked in Figure 8(b). Figure 8(c) shows the morphology of CFZs in $\text{N}_{0.5-2\#}$ specimen. As the plastic strain reached 1.0%, the precipitate free zones (PFZs) formed along the grain boundaries, as shown in Figure 8(d). Here, neither carbides nor γ' phase existed to pin the grain boundary. At 5.0% plastic strain, the M_6C carbides disappeared along the grain boundaries area. The microstructure along the grain boundary consisted of carbide chains, CFZs and PFZs, where the PFZs were more extended than that under the plastic strain of 1.0%. Figure 8(e) demonstrates the morphology of PFZs in $\text{N}_{5.0-2\#}$ specimen and the corresponding line scanning results from SEM-EDS. The element distribution of PFZs was close to the adjacent γ matrix, which was enriched in Cr and depleted in Ni and Al.

The grain boundary microstructure could be divided into four types: (1) MC carbide chains (mainly MC carbides); (2) fine M_6C carbides; (3) CFZs and (4) PFZs. Figure 9 shows the quantitative results of the linear density of typical microstructure along the grain boundary in DZ125 superalloy after the interrupted thermal cycling creep with different plastic strains. The linear density of MC carbide chains along the grain boundary consistently remained at 40%~50% during the creep. The linear density of fine M_6C carbides was reduced significantly at first and remained below 10% after reaching 0.5% plastic strain. With increasing the strain, the linear density of CFZs increased during the decelerating stage, remained at $\sim 40\%$ during the slow accelerating stage and decreased during the rapid accelerating stage. The linear density of PFZs increased with the strain following its appearance at 1.0% strain, especially during the rapid accelerating stage.



340 Figure 8—Typical microstructure along the grain boundary area of DZ125 superalloy after the
 interrupted thermal cycling creep with different plastic strains: (a) fine M_6C carbides in $N_{0.1-}$
 342 2# specimen, (b) carbide chains and carbides free zones (CFZs) in $N_{0.1-2\#}$ specimen, (c)
 carbides free zones (CFZs) in $N_{0.5-2\#}$ specimen, (d) precipitate free zones (PFZs) in $N_{1.0-2\#}$
 344 specimen, (e) the morphology of the PFZs along the grain boundary in $N_{5.0-2\#}$ specimen and

the corresponding SEM-EDS line scan results.

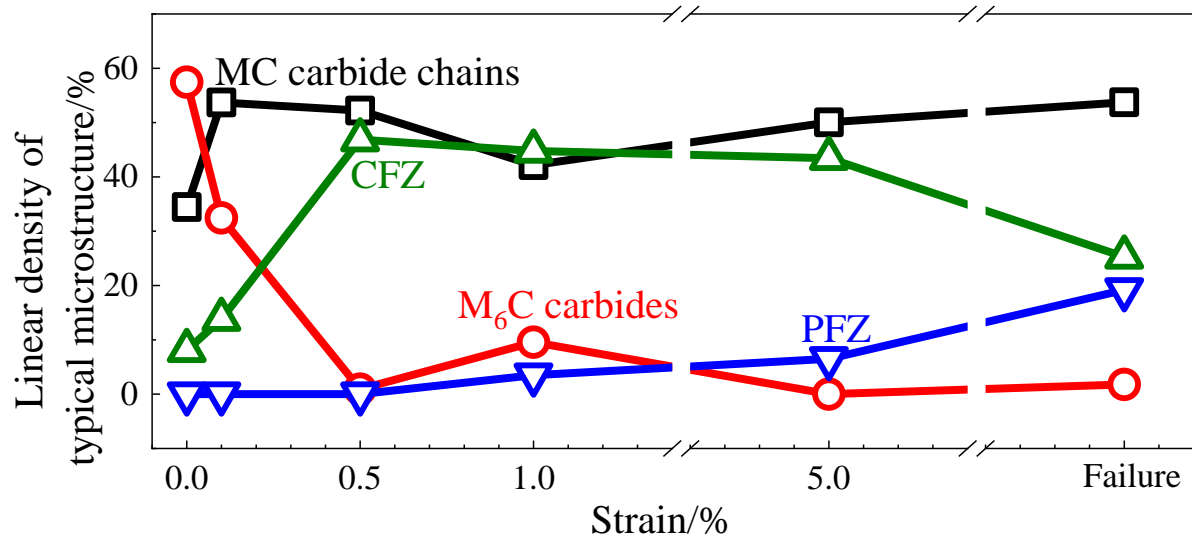


Figure 9—The linear density of the typical microstructure along the grain boundary of DZ125 superalloy after the interrupted thermal cycling creep tests at the 2# location with different plastic strains.

3.3. Substructural evolution during the thermal cycling creep

The dislocation configurations were observed for each interrupted creep specimen. Figure 10 shows the dislocation configurations in the primary dendrite core on the cross section of DZ125 superalloy after the interrupted thermal cycling creep with 0.1% plastic strain. Figure 10(a) demonstrates that few dislocations were gliding in the γ matrix, tangling and being pinned by the γ/γ' interface in N_{0.1}-1# specimen. The dislocation lines mostly aligned along the [100] and [110] directions, as marked by the black arrows. Figure 10(b) shows some randomly oriented dislocations in N_{0.1}-2# specimen which climbed over the γ' phase, as marked by the black arrows. The dislocation configuration of N_{0.1}-3# specimen was similar to that of N_{0.1}-1# specimen, as shown in Figure 10(c). As marked by the black arrows, more dislocations with the [010] direction appeared and were gliding towards the γ/γ' interface. Meanwhile, the randomly oriented dislocations with climbing characters were reduced. Figure 10 indicates that the dislocation configurations in the different locations of the thermal cycle under the decelerating stage were analogous.

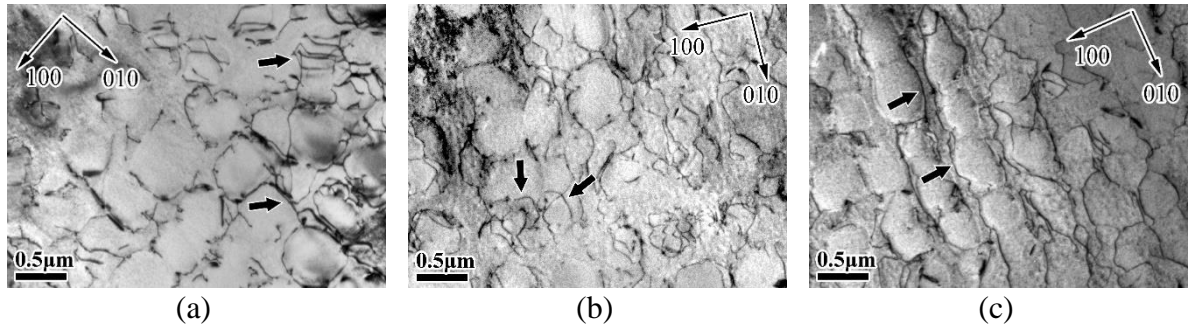


Figure 10—The dislocation configurations in the dendrite core of DZ125 superalloy after the interrupted thermal cycling creep with 0.1% plastic creep strain on the cross section: (a) N_{0.1}-1#, (b) N_{0.1}-2# and (c) N_{0.1}-3# specimen, $B \approx [001]/g=200$. The dislocations aligning along the [100] and [110] directions, climbing over the γ' phase, aligning along the [010] direction and gliding towards the γ/γ' interface are marked by the black arrows in (a), (b) and (c), respectively.

Figure 11 displays the dislocation configurations in the primary dendrite core of DZ125 superalloy after the interrupted thermal cycling creep with 0.5% plastic strain. The dislocation networks were observed in N_{0.5}-2# specimen, as shown in Figure 11(a). Figure 11(b) shows that some dislocations sheared the γ' phase at the concave interfaces and exhibit “zig-zag” character, as marked by the black arrow.

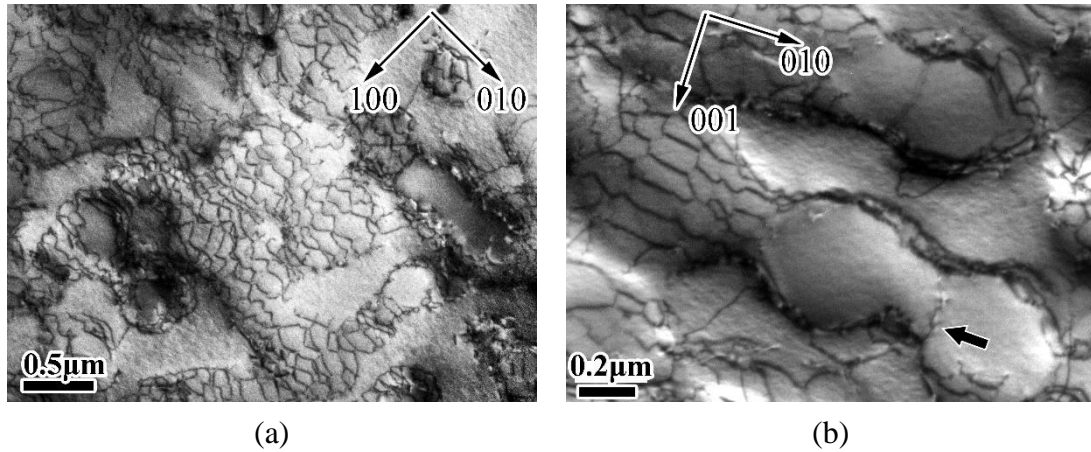


Figure 11—The dislocation configurations in the primary dendrite core of DZ125 superalloy after the interrupted thermal cycling creep of N_{0.5}-2# specimen: (a) dislocation networks, cross section, $B \approx [001]/g=200$; (b) dislocations sheared the γ' phase, longitudinal section, $B \approx [100]/g=020$. The dislocation shearing the γ' phase is marked by the black arrow in (b)

Figure 12 shows the dislocation configurations in the primary dendrite core of DZ125 superalloy after the interrupted thermal cycling creep with 1.0% plastic strain. Figure 12(a)

demonstrates the dislocation configurations on the cross section of N_{1.0}-1# specimen. Well-developed interfacial dislocation networks formed, and some dislocations sheared the γ' phase at the concave interfaces, as marked by the black arrows. The dislocation configurations of N_{1.0}-2# and N_{1.0}-3# specimens were analogous to that of N_{1.0}-1# specimen. Notably, the dislocation networks were more extended and covered a wider area in N_{1.0}-2# specimen than those in the other two specimens (images not shown here). Figure 12(b) depicts the dislocation configurations on the longitudinal section of N_{1.0}-1# specimen. The dislocations piled up at the γ/γ' interfaces perpendicular to the [001] direction. Some dislocations were trapped at the concave positions of the γ/γ' interfaces (white arrow in Figure 12(b)). Some of them even cut into the γ' phase, as marked by the black arrow in Figure 12(b). Figure 12(c) shows the dislocation configurations of N_{1.0}-2# specimen. A significant amount of dislocations sheared the γ' phase, crossed the entire rafted γ' precipitate and connected with the dislocation networks on both sides of the γ' precipitate, as marked by the black arrow.

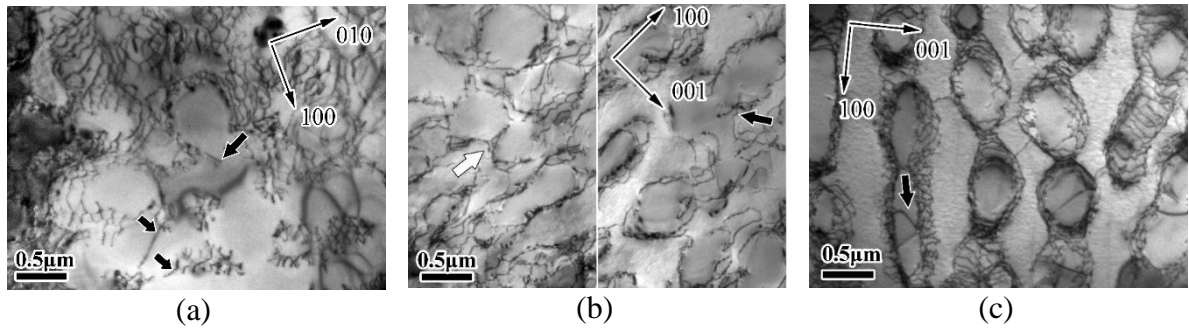


Figure 12—TEM images of dislocation configurations in the primary dendrite core of DZ125 superalloy after the interrupted thermal cycling creep with 1.0% plastic creep strain: (a) N_{1.0}-1# specimen, cross section, $\mathbf{B} \approx [001]/\mathbf{g} = 200$; (b) N_{1.0}-1# specimen, longitudinal section, $\mathbf{B} \approx [010]/\mathbf{g} = 002$; (c) N_{1.0}-2# specimen, longitudinal section, $\mathbf{B} \approx [010]/\mathbf{g} = 200$. The dislocations shearing the γ' phase are marked by the black arrows in (a), (b) and (c). The dislocation trapped at the concave positions of the γ/γ' interface is marked by the white arrow in (b).

Figure 13 shows the dislocation configurations in the primary dendrite core on the cross section of DZ125 superalloy after the interrupted thermal cycling creep with 5.0% plastic strain. The dislocation configurations at different thermal cycle locations were comparable under 5.0% plastic strain. The dislocation networks under 5.0% plastic strain were denser and more regular than those under 1.0% plastic strain. Most notably, more superdislocations sheared the γ' phase than that under 1.0% plastic strain. Some superdislocations were embedded inside the γ' phase, as marked by the black arrows in Figure 13. Some dislocations appeared to be bowed-out inside

the γ' phase, as marked by the white arrows in Figure 13. Among them, the bending in the superdislocation of N_{5.0}-2# specimen was more prominent.

Table 3 also lists the average dislocation network spacing of the interrupted creep specimens. The dislocation networks were firstly observed near the minimum creep rate (0.5% plastic strain), and their average spacing was ~ 95 nm. During the subsequent creep stages, the density of dislocation networks was similar at different thermal cycle locations under the same plastic strain. The average dislocation network spacing was 95 nm at the slow accelerating stage (1.0% plastic strain), which is close to that under 0.5% plastic strain. At the rapid accelerating stage (5.0% plastic strain), the dislocation networks were denser than those under 1.0% plastic strain, with an average dislocation network spacing of ~ 70 nm.

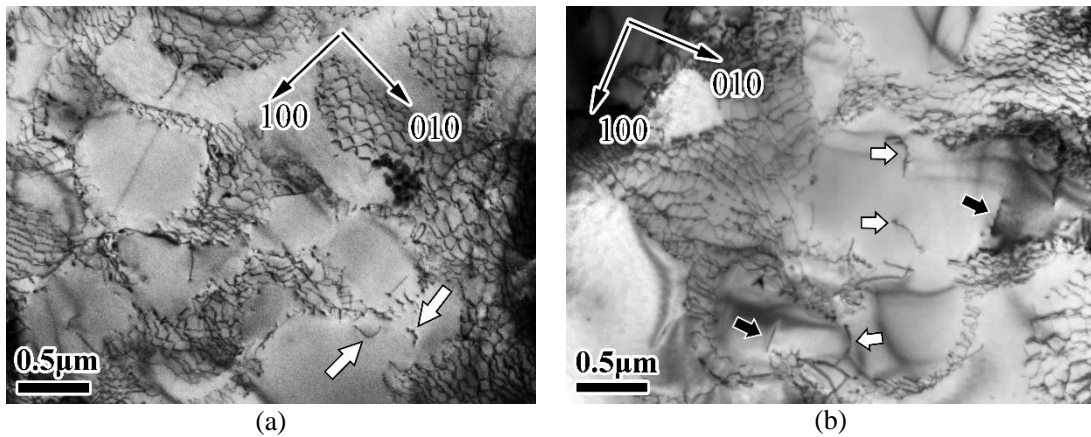


Figure 13—TEM images of dislocation configurations in the primary dendrite core of DZ125 superalloy after the interrupted thermal cycling creep with 5.0% plastic creep strain on the cross section: (a) N_{5.0}-1# and (b) N_{5.0}-2# specimens, $\mathbf{B} \approx [001]/\mathbf{g} = 200$. The dislocations embedded inside the γ' phase are marked by the black arrows. The dislocations bowed-out inside the γ' phase are marked by the white arrows.

4. Discussions

Thermal cycling creep of SX, DS and CC superalloys has been confirmed to be substantially influenced by overheating and the thermal cycling in previous studies^[4, 7, 9, 11, 22, 28]. As shown in our previous work^[22], the thermal cycling creep of DZ125 superalloy exhibits three distinct creep stages, with the minimum creep rate appearing earlier than that under the isothermal creep. Meanwhile, the majority of plastic deformation occurs during the overheating stage of the thermal cycle. In the following section, the microstructural and substructural evolutions in DZ125 superalloy during different thermal cycling creep stages will be analyzed

to reveal the creep mechanism. The difference of creep characters in three types of superalloys will be discussed.

4.1. Deformation mechanisms during the thermal cycling creep

(1) Decelerating stage

Under the isothermal creep at high-temperature and low-stress of superalloys, the original cuboidal γ' precipitates coarsen and coalesce during the first stage. Few dislocations glide and multiply in the γ matrix[29, 30], spread to the dislocation-free regions, then climb over the γ' precipitates when reaching the γ/γ' interfaces, together with the increasing creep strain[30]. The constantly increasing dislocations act as an effective hindrance to the subsequent dislocation movements[31]. Consequently, combined with the considerable Orowan resistance provided by the narrow γ channels[32], the creep strain rate decreases with the prolonged creep time until the minimum creep rate accompanied by the formation of rafted γ' microstructure.

In this study, the microstructural and substructural evolution of DZ125 superalloy during the decelerating stage of the thermal cycling creep were basically similar to those under the isothermal creep. In addition, the overheating and thermal cycling promoted further degeneration of the γ' phase[22] and earlier formation of the dislocation networks[7]. The 1100 °C stages resulted in a rapid decrease in γ' volume fraction from the original 67.6% to ~48%(Figure 3, Table 3), which is significantly lower than the equilibrium value at 950 °C (63.7%, Ref.[22]), slightly higher than that at 1100 °C (39.5%, Ref.[22]) and very close to that at 1050 °C (49.3%, Ref.[22]). Thus, it is indicated that the γ' phase was always in an unstable state during this type of thermal cycles, as suggested earlier by Giraud et al.[9] and Schwalbe et al.[12] for SX superalloys. Although it has been demonstrated that the γ' volume fraction can be recovered up to a higher value at the lower temperature stages than that at overheating temperature stage during the thermal cycling creep of SX superalloy AM1[5, 13], the γ' volume fraction barely recovered at the lower temperature stages in this study (more details were attached in Section 4.2). The γ' volume fraction of DZ125 superalloy remained at 45%~49% during the entire creep regime (Table 3, Figure 7).

During the decelerating stage of thermal cycling creep, the narrow γ channels as well as the gradually tangled dislocations provided strong hindrance to the gliding dislocations, then the spreading dislocations interacted with the γ' precipitates by climbing process (Figure 10). On this basis, the overheating stages further promoted the dislocation multiplying and moving in γ channels, and more obvious climbing events occurred (Figure 10(b)). Finally, the creep strain rate decreased gradually during the decelerating stage under thermal cycling creep with

the similar mechanism under the isothermal creep (Figure 2(b)), where the 1100 °C stages facilitated the further deformation and rapid strain accumulation.

The grain boundary microstructure also played an essential role in the creep deformation. The initial grain boundary microstructure of DZ125 superalloy includes the MC carbide chains (mainly consisted of MC carbides with slightly distributed M_6C carbides), fine M_6C carbides and a few carbides free zones (CFZs) (Ref.[22], Figure 9). The presence of discrete carbides along the grain boundaries could inhibit sliding during creep[1]. Since the solvus temperature of the MC carbides is higher than 1100 °C and the M_6C carbides will dissolve at <1100 °C[27], the fine M_6C carbides tended to dissolve and transform into CFZs during the 1100 °C stages. Nevertheless, the linear density of the MC carbide chains nearly remained constant during thermal cycling creep despite the slightly dissolved M_6C carbides (Figure 9). The reduction in carbide content and increased CFZs caused damage to the creep resistance of the grain boundaries by possibly favoring easier grain boundary sliding.

Figure 14(a) gives the schematic of the microstructure and substructure during the decelerating stage. Overall, the creep process during the decelerating stage under thermal cycling creep of DZ125 superalloy was similar to that under the isothermal creep[30, 33]. The original cuboidal γ' precipitates coarsened and coalesced; meanwhile the dislocations multiplied in the matrix and moved by the glide-climb process (Figure 3, Figure 10). The overall linear density of the carbides along the grain boundary reduced while the linear density of CFZs increased (Figure 9), giving rise to the degenerated grain boundary strength. The overheating stages accelerated the microstructural degradation and dislocation movements.

(2) Slow accelerating stage

Under the isothermal creep at high-temperature and low-stress of superalloys, the γ' precipitates tend to coarsen into the rafted γ' microstructure, and dense dislocation networks form together with severe dislocations climbing and shearing the γ' precipitates during the second stage[30, 34-37]. The rafted γ' microstructure and dense dislocation networks can increase the creep resistance by hindering the dislocations moving[35, 38]. Meanwhile, the dislocations shearing the γ' phase promote the further deformation of superalloys[39] by resulting in the annihilation of interfacial dislocations[39, 40].

In this study, the γ' volume fraction at the slow accelerating stage was slightly lower than that at the decelerating stage (Table 3, Figure 7). An early stage of the rafted γ' microstructure and dislocation networks formed near the minimum creep rate or the beginning of the slow accelerating stage ($N_{0.5-2\#}$ specimen, Figure 4(b), Figure 11(a)), which was accelerated by the overheating stages[22] and the thermal stress generated by the thermal cycling[41]. More

importantly, the dislocations began shearing the γ' phase near the minimum creep rate ($N_{0.5-2\#}$ specimen, Figure 11(b)).

The dislocations can shear the γ' phase more easily under the thermal cycling creep compared to the isothermal creep[15, 22]. Detailed explanations of this mechanism were given in the literatures[7, 15]. Even without loading stress, the thermal stress generated by each thermal cycle promoted dislocations shearing the γ' phase under the thermal fatigue tests of DZ125 superalloy [42]. In this study, the concave locations of the γ/γ' interface, resulting from the repeated “dissolution-precipitation” of the γ' phase, introduce a higher possibility for the dislocations shearing during the thermal cycling creep[15], which was also found in this study (Figure 11(b), Figure 12(b)). In addition, interfacial dislocations could be forced into the γ' phase because the interfacial area shrinks due to the γ' phase coalescing[7]. It can be inferred that the γ/γ' interfacial dislocation annihilation, induced by dislocations shearing the γ' phase in this study primarily occurred at the 1100 °C stages, as the dislocation activity was enhanced[28] and the γ' phase strength was weakened. The coupled effect of overheating and thermal cycling facilitated the dislocations shearing the γ' phase, reducing the creep resistance and increasing the creep rate in this stage.

During the slow accelerating stage, the M_6C carbides dissolved continuously and PFZs formed along the grain boundary. Two mechanisms were proposed to explain the cause of PFZs: (1) the directional diffusion of Cr towards the grain boundary area which is promoted by the applied creep stress[43, 44]; (2) the dragging or the dissolution of particles due to grain boundary sliding or migration[45]. In this study, it is demonstrated that the element distribution of PFZs was close to the adjacent γ matrix (Figure 8(e)). Thus, it can be assumed that the appearance of PFZs was mainly due to grain boundary sliding, which caused damage to the creep resistance of the grain boundary area.

Figure 14(b) gives the schematic of the microstructure and substructure during the slow accelerating stage. Overall, the γ' phase coarsened more seriously and directly coalesced into the rafting structure, and dense dislocation networks formed together with the dislocations shearing the γ' phase during the slow accelerating stage. Meanwhile, PFZs appeared along the grain boundary. The combining effect of CFZs and PFZs impaired the creep resistance. The overheating and thermal cycling process promoted dislocations shearing the γ' phase. Under the coupled effect of the above microstructure features, the creep rate increased slowly with increasing the strain.

(3) Rapid accelerating stage

Under the isothermal creep at high-temperature and low-stress of superalloys, the

predominant microstructural features of the third stage include well-developed rafted γ' microstructure and dislocation networks, wider γ channels[40] and a significant number of dislocations shearing the γ' phase[46]. Consequently, the creep strain rate increases rapidly with prolonged creep time. Meanwhile, cracks are initiated at carbides, γ/γ' eutectic pools and grain boundaries, which result in the fracture[46, 47].

In this study, the γ' volume fraction reduced slightly during the rapid accelerating stage compared to those of the previous stages (Table 3, Figure 7). The γ' phase coarsened and coalesced more severely into the rafting structure (Figure 6), and the γ channels became wider (Table 3, Figure 7). The dislocation networks tended to be denser and more regular than those at the slow accelerating stage (Figure 12, Figure 13, Figure 7). Meanwhile, more dislocations sheared the γ' phase and superdislocations inside the γ' phase were bowed-out, especially during the 1100 °C stages (Figure 13(b)), related to the deformation of the γ' phase. Viguier et al.[28] suggested that the density of superdislocations was probably the crucial parameter to control the creep rate instead of the climb velocity.

During the rapid accelerating stage, the linear density of the PFZs increased and the linear density of CFZs decreased (Figure 9). A dispersed distribution of carbides along the grain boundaries can pin the grain boundaries from sliding[1, 48-50], therefore, the grain boundaries with CFZs would deform more easily and transform into PFZs. Meanwhile, more cracks initiated along the grain boundaries, carbides and γ/γ' eutectic pools as indicated by the previous work[22], in comparison with that under the isothermal creep.

Figure 14(c) depicts the microstructure and substructure during this stage. Overall, the γ' phase in DZ125 superalloy coarsened and coalesced more severely, while the creep resistance of grain boundaries decreased during the rapid accelerating stage. The predominant deformation mechanism was the significant increased number of dislocations shearing into the γ' phase, which is also similar to the isothermal creep within the final creep stage. The overheating and thermal cycling process promoted the formation of PFZs and cracks. Under the coupled effect of the above microstructure features, the creep rate increased rapidly with increasing strain.

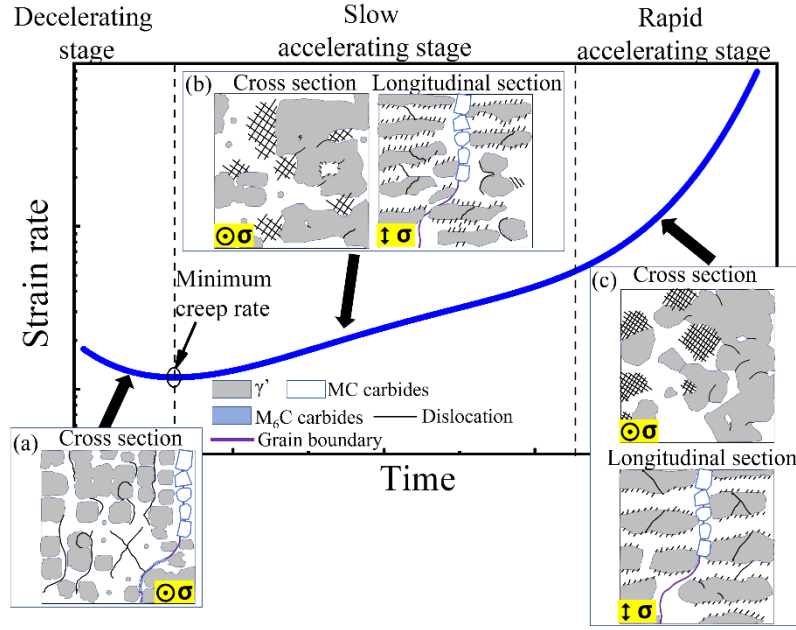


Figure 14—Schematic illustration of the thermal cycling creep in DZ125 superalloy: (a) decelerating stage, (b) slow accelerating stage and (c) rapid accelerating stage.

4.2. Thermal cycling effect on γ' volume fraction

During the thermal cycling creep, the γ' phase in SX superalloys[5, 13] and CC superalloys[15] dissolves during the overheating stages and then recovers substantially during the lower temperature stages. For example, the γ' volume fraction of AM1 superalloy (SX) reduces to ~54% at the overheating temperature stage (1100 °C) and effectively recovers to ~65% after holding at the lower temperature stage (1010 °C) for a few minutes[5, 7]. However, the γ' volume fraction in DZ125 superalloy hardly recovered during the lower temperature stages (Table 3, Figure 7).

Similar to the coarsening of the γ' phase which is affected by the elemental diffusion in the γ matrix[51], the recovery of the γ' phase at the lower temperature stages also depends on the effective diffusivity D_{eff} . The effective diffusivity D_{eff} at temperature T can be described as[52]:

$$D_{eff} = D_0^{eff} \exp \left(-\frac{Q_{eff}}{RT} \right) \quad (1)$$

where R is the gas constant, T is the absolute temperature, D_0^{eff} is the pre-exponential factor and Q_{eff} is the effective activation energy. The value of D_0^{eff} can be estimated as[52]:

$$D_0^{eff} = \frac{1}{\sum_m \frac{x_m}{D_0^{m,Ni}}} \quad (2)$$

where x_m is the solute concentration of element m in the γ matrix and $D_0^{m,Ni}$ is the diffusion coefficient of element m in pure Nickel.

Q_{eff} is defined according to Ref.[52] as:

$$Q_{eff} = \sum_m x_m Q_{m,Ni} \quad (3)$$

where $Q_{m,Ni}$ is the activation energy for the interdiffusion of solute m in pure Nickel.

In this study, the solute concentration of element m in the γ matrix (x_m) of DZ125 and AM1 superalloys are given in Table 4. The diffusion coefficient ($D_0^{m,Ni}$) and activation energy for the interdiffusion ($Q_{m,Ni}$) of solute m are listed in Table 5, and they are taken from the Refs.[53-57]. Consequently, the estimated effective diffusivity D_{eff} of AM1 superalloy at 1010 °C is calculated to be $5.09 \times 10^{-16} m^2 s^{-1}$, which is obviously higher than that of DZ125 superalloy at 950 °C, $1.22 \times 10^{-16} m^2 s^{-1}$. Therefore, when considering the thermal cycling creep of AM1 superalloy under the condition of 1010 °C~1100 °C, the γ' volume fraction could recover during the 1010 °C stage in a few minutes[5, 7] due to the faster elemental diffusion, whereas the recovery of the γ' volume fraction in DZ125 superalloy is more sluggish at 950 °C stage.

It should be pointed out that the fine secondary γ' precipitates in the γ matrix, as shown in Figure 3-6, were not involved in the above discussion, which should be the result of unrecovered γ' volume fraction during the lower temperature stages and would dissolve during the heating and 1100 °C holding stages. Since the 1100 °C holding stages were the predominant stages for creep deformation, those fine secondary γ' precipitates in the γ matrix would slightly affect the creep property of the alloy during thermal cycling creep.

4.3. Characteristics and creep damage of different types of superalloys

Based on the previous researches of the thermal cycling creep on SX, CC and DS superalloys, some differences and similarities can be deduced. For the SX superalloy, plastic deformation mainly occurred during the overheating stages[11]. Compared to the isothermal creep, the thermal cycling creep exhibited unique features such as shorter creep life[9], higher creep strain rate[9] and higher fracture strain[23]. The primary cause of the shorter creep life was the significant reduction of the γ' volume fraction during the overheating stages[11, 23], resulting in easy deformation. Meanwhile, the thermal cycling also accelerated the formation of the rafted γ' microstructure and dislocation networks[12]. Few investigations on the creep mechanisms at various thermal cycle creep stages were reported. Schwalbe et al.[12] revealed that the accelerating creep rate was related to dislocations shearing the γ' phase after the

minimum creep rate. Meanwhile, rarely studies on the carbides were published due to the absence or lower carbon content in SX superalloys, but Antonov et al.[23] found that the carbides were the main crack initiation sites in SX superalloy Rene N5. Failure specimens possessed more cracks and voids under the thermal cycling creep than those under the isothermal creep, which result in a higher fracture strain[23].

Table 4—Measured chemical compositions of elements in γ phase of DZ125[58] superalloy and AM1 superalloy[59] (at. %)

Element	Ni	Co	Cr	Al	Mo	W	Ta	Ti
DZ125	51.48	17.27	22.81	3.77	2.08	2.22	0.11	0.19
AM1	53.90	11.10	26.10	3.00	2.50	2.30	0.70	0.40

Note: *The composition of DZ125 superalloy was measured by physic-chemical phase analysis and referred to Ref.[58]. The composition of AM1 superalloy was measured by atom probe tomography and referred to the Ref.[59].

Table 5— $D_0^{Ni,m}$ and $Q_{Ni,m}$ for the interdiffusion of elements in Ni

Element	$D_0^{Ni,m}(m^2/s)$	$Q_{Ni,m}(kJ/mol)$	Refs.
Ni	1.90×10^{-4}	284.00	[53]
Co	7.50×10^{-5}	285.10	[53]
Cr	3.00×10^{-6}	170.70	[53]
Al	1.00×10^{-3}	272.09	[54]
Mo	1.15×10^{-4}	281.30	[55]
Ta	2.19×10^{-5}	251.00	[56]
W	8.00×10^{-6}	264.00	[56]
Ti	4.10×10^{-4}	275.00	[57]

For the CC superalloys, similar features of creep properties as well as microstructural and substructural evolutions were revealed compared with these under the isothermal creep and even those for SX superalloys[14, 15]. Nevertheless, CC superalloys were more affected by the presence of carbides and grain boundaries than SX superalloys. Carbide evolution was observed under both the thermal cycling[15] and isothermal creep[60], such as the MC carbides degenerating into M_6C carbides. The thermal stress induced by the temperature cycling promoted the crack initiation at the carbide interfaces and grain boundaries in CC superalloys[15]. The higher fracture strain under the thermal cycling creep was mainly due to more cracks and creep voids in CC superalloys and the cracks propagated along the grain boundaries, leading to the intergranular fracture[14, 15].

The DS superalloy DZ125 exhibited macroscopical thermal cycling creep characteristics such as shorter creep life, slightly lower strain rate, earlier appearance of minimum creep rate

and no difference in fracture strain compared with characteristics of the isothermal creep[22]. The microstructural and substructural characteristics of DZ125 superalloy were basically similar to those of SX and CC superalloys, with one distinction that the γ' volume fraction did not recover during the low temperature stages. In addition, it was demonstrated that the final fracture mode was still transgranular fracture in the thermal cycling creep of DZ125 superalloy in our previous research[22], which was different from CC superalloys.

As a whole, overheating and thermal cycling are the two types of damage that can occur in all three types of superalloys. Overheating damage is caused by very high temperatures (usually within a very short time), which can accelerate microstructure degradation, such as γ' phase dissolution, carbide dissolution, dislocations climb and dislocations shearing the γ' phase. Thus, overheating reduces the precipitate strength while enhancing dislocation activity. While thermal cycling damage refers to damage caused by repeated changes in creep temperatures. Even in thermal fatigue testing without loading stress, the thermal stress induced by temperature changes can also cause γ' phase coarsening and rafting[41], dislocations multiplication, dislocation networks formation and dislocations shearing the γ' phase[42]. Meanwhile, the thermal stress also promotes crack initiation at the precipitate interface and grain boundaries[42]. During the thermal cycling creep, the coupled effect of overheating and thermal cycling can simultaneously promote the above microstructural and substructural evolution, thus ultimately accelerating the creep deformation.

5. Conclusions

In this study, a directionally solidified superalloy DZ125 was subjected to thermal cycling creep under (950 °C/15 min+1100 °C/1 min)-100 MPa, which exhibits different creep stages, including decelerating, slow accelerating and rapid accelerating stages. The evolution of the microstructure and dislocation configurations during different creep stages were investigated and the creep mechanisms were revealed. The main conclusions are summarized as follows:

(1) The 1100 °C stages caused significant γ' phase dissolution at the beginning of creep. The γ' volume fraction did not recover at the lower temperature of 950 °C due to the slow elemental diffusion. Therefore, the γ' volume fraction remained at ~45% during the entire creep process.

(2) During the decelerating stage, the original cuboidal γ' precipitates coarsened and coalesced. A few dislocations multiplied in the narrow γ channels and moved by the glide-climb process. The 1100 °C stages resulted in the dissolution of M_6C carbides and the formation

of CFZs (carbides free zones) along the grain boundaries, reducing the creep resistance. With increasing the plastic strain, the dislocations multiplied and the movement of dislocations was hindered, therefore the creep rate decreased gradually.

(3) During the slow accelerating stage, the rafted γ' microstructure and dislocation networks formed and could prevent further dislocation moving. In the meantime, the dislocations began to shear the γ' phase, which promoted the creep deformation and was facilitated by the overheating and thermal cycling process. In addition, PFZs (precipitate free zones) formed along the grain boundary and diminished the creep resistance. As a result, the creep rate kept increasing slowly after the minimum creep rate.

(4) During the rapid accelerating stage, the γ' phase coarsened and coalesced more severely into a more obvious rafted γ' microstructure with widening γ channels. Simultaneously, a large number of dislocations sheared the γ' phase. The CFZs along the grain boundaries transformed into PFZs due to the easier deformation at these locations, resulting in the increase of the linear density of PFZs. The degradation of the γ' phase and grain boundary reduced the creep resistance. Meanwhile, cracks initiated along the grain boundaries, carbides and γ/γ' eutectic pools, which was promoted by the thermal cycling process. Therefore, the creep rate accelerated rapidly.

Acknowledgements

The authors are grateful to Prof. Wangyue Yang and Dr. Yadong Chen for their professional advice and help. This work is supported by the National Science and Technology Major Project (J2019-VII-0010-0150), the National Natural Science Foundation of China (Grant No. 91860201), National Science and Technology Major Project (J2019-IV-0006-0074) and National Science and Technology Major Project (J2019-VII-0010-0150). Institut Pprime gratefully acknowledges Contrat de Plan Etat - Région Nouvelle-Aquitaine (CPER) as well as the Fonds Européen de Développement Régional (FEDER) for their partial financial support to the reported work.

- [1] T.M. Pollock, S. Tin, Nickel-based superalloys for advanced turbine engines: chemistry, microstructure and properties, *J. Propul. Power.* 22 (2006) 361-374.<https://doi.org/10.2514/1.18239>
- [2] X.T. Guo, W.W. Zheng, C.B. Xiao, L.F. Li, S. Antonov, Y.R. Zheng, Q. Feng, Evaluation of microstructural degradation in a failed gas turbine blade due to overheating, *Eng. Failure. Anal.* 103 (2019) 308-318.<https://doi.org/10.1016/j.engfailanal.2019.04.021>
- [3] J. Cormier, X. Milhet, F. Vogel, J. Mendez, Non-isothermal creep behavior of a second generation Ni-based single crystal superalloy: experimental characterization and modeling, in: R.C. Reed, K.A. Green, P. Caron, T.P. Gabb, M.G. Fahrman, E.S. Huron (Eds.) *Superalloys 2008: Proceedings of the 11th International Symposium of Superalloys*, The Minerals, Metals & Materials Society (TMS), Seven Springs, Champion, Pennsylvania, USA, 2008, pp. 941-949
- [4] A. Raffaitin, D. Monceau, F. Crabos, E. Andrieu, The effect of thermal cycling on the high-temperature creep behaviour of a single crystal nickel-based superalloy, *Scripta. Mater.* 56 (2007) 277-280.<https://doi.org/10.1016/j.scriptamat.2006.10.026>
- [5] J.-B. Le Graverend, L. Dirand, A. Jacques, J. Cormier, O. Ferry, T. Schenk, F. Gallerneau, S. Kruch, J. Mendez, In situ measurement of the γ/γ' lattice mismatch evolution of a Nickel-based single-crystal superalloy during non-isothermal very high-temperature creep experiments, *Metall. Mater. Trans. A.* 43A (2012) 3946-3951.<https://doi.org/10.1007/s11661-012-1343-x>
- [6] S. Steuer, Z. Hervier, S. Thabart, C. Castaing, T.M. Pollock, J. Cormier, Creep behavior under isothermal and non-isothermal conditions of AM3 single crystal superalloy for different solutioning cooling rates, *Mat. Sci. Eng. A.* 601 (2014) 145-152.<https://doi.org/10.1016/j.msea.2014.02.046>
- [7] C. Schwalbe, J. Cormier, C. Jones, E. Galindo-Nava, C. Rae, Investigating the dislocation-driven micro-mechanical response under non-isothermal creep conditions in single-crystal superalloys, *Metall. Mater. Trans. A.* 49 (2018) 3988-4002.<https://doi.org/10.1007/s11661-018-4764-3>
- [8] J. Cormier, Thermal cycling creep resistance of Ni-based single crystal superalloys, in: M. Hardy, E. Huron, U. Glatzel, B. Griffin, B. Lewis, C. Rae, V. Seetharaman, S. Tin (Eds.) *Superalloys 2016: Proceedings of the 13th International Symposium of Superalloys*, John Wiley & Sons, Inc., Seven Springs, Champion, Pennsylvania, USA, 2016, pp. 383-394.<https://doi.org/10.1002/9781119075646.ch42>
- [9] R. Giraud, J. Cormier, Z. Hervier, D. Bertheau, K. Harris, J. Wahl, X. Milhet, J. Mendez, A. Organista, Effect of the prior microstructure degradation on the high temperature/low stress non-isothermal creep behavior of CMSX-4 (R) Ni-based single crystal superalloy, in: E.S. Huron, R.C. Reed, M.C. Hard, M.J. Mills, R.E. Montero, P.D. Portella, J. Telesman (Eds.) *Superalloys 2012: Proceedings of the 12th International Symposium on Superalloys*, John Wiley & Sons, Inc., Seven Springs, Champion, Pennsylvania, USA, 2012, pp. 265-274.<https://doi.org/10.1002/9781118516430.ch29>
- [10] J. Cormier, X. Milhet, J. Mendez, Non-isothermal creep at very high temperature of the nickel-based single crystal superalloy MC2, *Acta Mater.* 55 (2007) 6250-6259.<https://doi.org/10.1016/j.actamat.2007.07.048>
- [11] J. Cormier, M. Jouiad, F. Hamon, P. Villechaise, X. Milhet, Very high temperature creep behavior of a single crystal Ni-based superalloy under complex thermal cycling conditions, *Phil. Mag. Lett.* 90 (2010) 611-620.<https://doi.org/10.1080/09500839.2010.489887>
- [12] C. Schwalbe, A. Jacques, E. Galindo-Nava, C. Jones, C. Rae, J. Cormier, In situ measurement of the precipitate volume fraction and interfacial lattice misfit during non-isothermal creep in the superalloy CMSX-4, *Mat. Sci. Eng. A.* 740 (2019) 182-186.<https://doi.org/10.1016/j.msea.2018.10.033>
- [13] J.-B. le Graverend, A. Jacques, J. Cormier, O. Ferry, T. Schenk, J. Mendez, Creep of a nickel-based single-crystal superalloy during very high-temperature jumps followed by synchrotron X-ray diffraction, *Acta. Mater.* 84 (2015) 65-79.<http://dx.doi.org/10.1016/j.actamat.2014.10.036>
- [14] X.F. Yuan, W.R. An, Y.W. Ju, S. Antonov, Z.N. Bi, W. Li, J.T. Wu, Evaluation of microstructural degradation and its corresponding creep property in integral cast turbine rotor made of K424 alloy, *Mater.*

Charact. 158 (2019) 109946.<https://doi.org/10.1016/j.matchar.2019.109946>

[15] X.T. Guo, W.W. Zheng, W.R. An, S. Antonov, L.F. Li, J. Cormier, Q. Feng, High temperature creep behavior of a cast polycrystalline nickel-based superalloy K465 under thermal cycling conditions, *Materialia*. 14 (2020) 100913.<https://doi.org/10.1016/j.mtla.2020.100913>

[16] F.I. Versnyder, M.E. Shank, The development of columnar grain and single crystal high temperature materials through directional solidification, *Mat. Sci. Eng.* 6 (1970) 213-247.[https://doi.org/10.1016/0025-5416\(70\)90050-9](https://doi.org/10.1016/0025-5416(70)90050-9)

[17] R.C. Reed, *The superalloys: fundamentals and applications*, Cambridge university press, 2006

[18] J.C. Stinville, L.M. Suave, F. Mauget, L. Marcin, P. Villechaise, T.M. Pollock, J. Cormier, Damage nucleation during transverse creep of a directionally solidified Ni-based superalloy, *Mat. Sci. Eng. A.* (2022) 144089.<https://doi.org/10.1016/j.msea.2022.144089>

[19] L.M. Suave, J. Cormier, P. Villechaise, D. Bertheau, G. Benoit, F. Mauget, G. Cailletaud, L. Marcin, F. Futuroscope-Chasseneuil, High temperature creep damage mechanisms in a directionally solidified alloy: impact of crystallography and environment, in: M. Hardy, E. Huron, U. Glatzel, B. Griffin, B. Lewis, C. Rae, V. Seetharaman, S. Tin (Eds.) *Superalloys 2016: Proceedings of the 13th International Symposium of Superalloys*, John Wiley & Sons, Inc., Seven Springs, Champion, Pennsylvania, USA, 2016, pp. 745-756.<https://doi.org/10.1002/9781119075646.ch80>

[20] L. He, Q. Zheng, X. Sun, H. Guan, Z. Hu, A. Tieu, C. Lu, H. Zhu, Effect of carbides on the creep properties of a Ni-base superalloy M963, *Mat. Sci. Eng. A.* 397 (2005) 297-304.<https://doi.org/10.1016/j.msea.2005.02.038>

[21] S.G. Tian, N. Tian, H.C. Yu, X.L. Meng, Y. Li, Influence of solution temperature on microstructure and creep property of a directional solidified nickel-based superalloy at intermediate temperatures, *Mat. Sci. Eng. A.* 615 (2014) 469-480.<http://dx.doi.org/10.1016/j.msea.2014.07.103>

[22] W.R. An, S. Utada, X.T. Guo, S. Antonov, W.W. Zheng, J. Cormier, Q. Feng, Thermal cycling creep properties of a directionally solidified superalloy DZ125, *J. Mater. Sci. Technol.* 104 (2022) 269-284.<https://doi.org/10.1016/j.jmst.2021.07.015>

[23] S. Antonov, W.R. An, S. Utada, X.T. Guo, C. Schwalbe, W.W. Zheng, C.M.F. Rae, J. Cormier, Q. Feng, Evaluation and comparison of damage accumulation mechanisms during non-isothermal creep of cast Ni-based superalloys, in: S. Tin, M. Hardy, J. Clews, J. Cormier, Q. Feng, J. Marcin, C. O'Brien, A. Suzuki (Eds.) *Superalloys 2020: Proceedings of the 14th International Symposium of Superalloys*, Springer International Publishing, Cham, 2020, pp. 228-239.https://doi.org/10.1007/978-3-030-51834-9_22

[24] ASTM, Standard test method for determining volume fraction by systematic manual point count, in: *ASTM E562-19*, ASTM Int., PA, USA, 2019.<https://doi.org/10.1520/E0562-19>

[25] C. Fu, Y.D. Chen, L.F. Li, S. Antonov, Q. Feng, Evaluation of service conditions of high pressure turbine blades made of DS Ni-base superalloy by artificial neural networks, *Mater. Today. Commun.* 22 (2020) 100838.<https://doi.org/10.1016/j.mtcomm.2019.100838>

[26] J.Y. Tong, K. Yagi, Y.R. Zheng, Q. Feng, Microstructural degradation and its corresponding mechanical property of wrought superalloy GH4037 caused by very high temperature, *J. Alloy. Compd.* 690 (2017) 542-552.<https://doi.org/10.1016/j.jallcom.2016.08.081>

[27] Y.D. Chen, W.W. Zheng, Y.R. Zheng, Q. Feng, Microstructural evolution and corresponding stress rupture property in DZ125 alloy after thermal exposure. *Chin. J. Rare. Met.* 42 (2018) 1009-1017. <https://doi.org/10.13373/j.cnki.cjrm.xy17090026>

[28] B. Viguier, F. Touratier, E. Andrieu, High-temperature creep of single-crystal nickel-based superalloy: microstructural changes and effects of thermal cycling, *Phil. Mag.* 91 (2011) 4427-4446.<https://doi.org/10.1080/14786435.2011.609151>

[29] A. Epishin, T. Link, Mechanisms of high-temperature creep of nickel-based superalloys under low applied stresses, *Phil. Mag.* 84 (2004) 1979-2000.<https://doi.org/10.1080/14786430410001663240>

[30] J.X. Zhang, J.C. Wang, H. Harada, Y. Koizumi, The effect of lattice misfit on the dislocation motion in superalloys during high-temperature low-stress creep, *Acta. Mater.* 53 (2005) 4623-4633.<https://doi.org/10.1016/j.actamat.2005.06.013>

[31] J.X. Zhang, T. Murakumo, H. Harada, Y. Koizumi, Dependence of creep strength on the interfacial

dislocations in a fourth generation SC superalloy TMS-138, *Scripta. Mater.* 48 (2003) 287-293.[http://dx.doi.org/10.1016/S1359-6462\(02\)00379-2](http://dx.doi.org/10.1016/S1359-6462(02)00379-2)

[32] T.M. Pollock, A.S. Argon, Creep resistance of CMSX-3 nickel base superalloy single crystals, *Acta Metallurgica et Materialia*, 40 (1992) 1-30. [https://doi.org/10.1016/0956-7151\(92\)90195-K](https://doi.org/10.1016/0956-7151(92)90195-K)

[33] W.S. Xia, X.B. Zhao, L. Yue, Z. Zhang, Microstructural evolution and creep mechanisms in Ni-based single crystal superalloys: A review, *J. Alloy. Compd.* 819 (2020) 152954. <https://doi.org/10.1016/j.jallcom.2019.152954>

[34] Q.Y. Shi, J.J. Huo, Y.R. Zheng, Q. Feng, Influence of Mo and Ru additions on the creep behavior of Ni-based single crystal superalloys at 1100° C, *Mat. Sci. Eng. A.* 725 (2018) 148-159. <https://doi.org/10.1016/j.msea.2018.04.026>

[35] X.P. Tan, J.L. Liu, T. Jin, Z.Q. Hu, H.U. Hong, B.G. Choi, I.S. Kim, C.Y. Jo, D. Mangelinck, Effect of Ru additions on very high temperature creep properties of a single crystal Ni-based superalloy, *Mat. Sci. Eng. A.* 580 (2013) 21-35. <https://doi.org/10.1016/j.msea.2013.05.028>

[36] X.G. Wang, J.L. Liu, T. Jin, X.F. Sun, Z.Q. Hu, J.H. Do, B.G. Choi, I.S. Kim, C.Y. Jo, Dislocation motion during high-temperature low-stress creep in Ru-free and Ru-containing single-crystal superalloys, *Mater. Design.* 67 (2015) 543-551. <http://dx.doi.org/10.1016/j.matdes.2014.11.002>

[37] X. Milhet, M. Arnoux, J. Cormier, J. Mendez, C. Tromas, On the influence of the dendritic structure on the creep behavior of a Re-containing superalloy at high temperature/low stress, *Mat. Sci. Eng. A.* 546 (2012) 139-145. <http://dx.doi.org/10.1016/j.msea.2012.03.041>

[38] F.R. Nabarro, Rafting in superalloys, *Metall. Mater. Trans. A.* 27 (1996) 513-530. <https://doi.org/10.1007/BF02648942>

[39] P.M. Sarosi, R. Srinivasan, G.F. Eggeler, M.V. Nathal, M.J. Mills, Observations of a $\langle 010 \rangle$ dislocations during the high-temperature creep of Ni-based superalloy single crystals deformed along the $[001]$ orientation, *Acta. Mater.* 55 (2007) 2509-2518. <https://doi.org/10.1016/j.actamat.2006.11.045>

[40] R. Srinivasan, G.F. Eggeler, M.J. Mills, γ' -cutting as rate-controlling recovery process during high-temperature and low-stress creep of superalloy single crystals, *Acta. Mater.* 48 (2000) 4867-4878. [https://doi.org/10.1016/S1359-6454\(00\)00292-5](https://doi.org/10.1016/S1359-6454(00)00292-5)

[41] J.X. Yang, Q. Zheng, X.F. Sun, H.R. Guan, Z.Q. Hu, Morphological evolution of γ' phase in K465 superalloy during thermal fatigue, *Tran. Nonferrous Met. Soc. Chin (English Edition)*, 16 (2006) 1986-1989

[42] J.L. Zhang, Z.H. Zhao, Y.H. Kong, Z. Zhang, Q.P. Zhong, Crack initiation and propagation mechanisms during thermal fatigue in directionally solidified superalloy DZ125, *Int. J. Fatigue.* 119 (2019) 355-366. <https://doi.org/10.1016/j.ijfatigue.2018.09.001>

[43] L. Wang, G. Xie, J. Zhang, L.H. Lou, Precipitate free zones along recrystallization grain boundaries during creep in a directionally solidified superalloy, *Mater. Sci. Forum.* 546-549 (2007) 1235-1240. <http://www.scientific.net/MSF.546-549.1235>

[44] S. Komazaki, T. Shoji, Formation of the Al-rich phase on grain boundary and the creep damage mechanism in directionally solidified Ni-base superalloy, *Metall. Mater. Trans. A.* 28 (1997) 1945-1949. <https://doi.org/10.1007/s11661-997-0125-3>

[45] J.M. Doh, K.K. Yoo, H.K. Baik, J. Choi, S.K. Hur, Effect of creep stress on microstructure of a Ni-Cr-W-Al-Ti superalloy, *Scripta. Mater.* 34 (1996) 537-542. [https://doi.org/10.1016/1359-6462\(95\)00562-5](https://doi.org/10.1016/1359-6462(95)00562-5)

[46] Y.W. Li, L. Wang, G. Zhang, W. Zheng, L.H. Lou, J. Zhang, On the role of topological inversion and dislocation structures during tertiary creep at elevated temperatures for a Ni-based single crystal superalloy, *Mat. Sci. Eng. A.* 809 (2021) 140982. <https://doi.org/10.1016/j.msea.2021.140982>

[47] P. Caron, C. Ramusat, F. Diologent, Influence of the γ' fraction on the γ/γ' topological inversion during high temperature creep of single crystal superalloys, in: R.C. Reed, K.A. Green, P. Caron, T.P. Gabb, M.G. Fahrman, E.S. Huron (Eds.) *Superalloys 2008: Proceedings of the 11th International Symposium of Superalloys*, The Minerals, Metals & Materials Society (TMS), Seven Springs, Champion, Pennsylvania, USA, 2008,

[48] Y.L. Xu, Q.M. Jin, X.S. Xiao, X.L. Cao, G.Q. Jia, Y.M. Zhu, H.J. Yin, Strengthening mechanisms of carbon in modified nickel-based superalloy Nimonic 80A, *Mat. Sci. Eng. A.* 528 (2011) 4600-4607. <https://doi.org/10.1016/j.msea.2011.02.072>

- [49] Q.Z. Chen, C.N. Jones, D.M. Knowles, The grain boundary microstructures of the base and modified RR 2072 bicrystal superalloys and their effects on the creep properties, *Mat. Sci. Eng. A.* 385 (2004) 402-418.<https://doi.org/10.1016/j.msea.2004.07.013>
- [50] H. Tanaka, M. Murata, F. Abe, K. Yagi, The effect of carbide distributions on long-term creep rupture strength of SUS321H and SUS347H stainless steels, *Mat. Sci. Eng. A.* 234-236 (1997) 1049-1052.[https://doi.org/10.1016/S0921-5093\(97\)00360-2](https://doi.org/10.1016/S0921-5093(97)00360-2)
- [51] J. Lapin, M. Gebura, T. Pelachová, M. Nazmy, Coarsening kinetics of cuboidal γ' precipitates in single crystal nickel base superalloy CMSX-4, *Kovove Mater.* 46 (2008) 313-322
- [52] C. Ai, X.B. Zhao, J. Zhou, H. Zhang, L. Liu, Y.L. Pei, S.S. Li, S.K. Gong, Application of a modified Ostwald ripening theory in coarsening of γ' phases in Ni-based single crystal superalloys, *J. Alloy. Compd.* 632 (2015) 558-562.<https://doi.org/10.1016/j.jallcom.2015.01.215>
- [53] Z. Zhu, H. Basoalto, N. Warnken, R. Reed, A model for the creep deformation behaviour of Nickel-based single crystal superalloys, *Acta. Mater.* 60 (2012) 4888-4900.<https://doi.org/10.1016/j.actamat.2012.05.023>
- [54] M. Janssen, Diffusion in the nickel-rich part of the nickel-aluminum system at 1000 to 1300 deg. Nickel-Aluminum (Ni₃Al) layer growth, diffusion coefficients, and interface concentrations, *Metall. Trans.* 4 (1973) 1623-1633.<https://doi.org/10.1007/BF02668017>
- [55] M. Karunaratne, R. Reed, Interdiffusion of Niobium and Molybdenum in Nickel between 900-1300 °C, in: *Defect and Diffusion forum*, Trans Tech Publications Ltd, 2005, pp. 420-425
- [56] M.S.A. Karunaratne, P. Carter, R.C. Reed, Interdiffusion in the face-centred cubic phase of the Ni-Re, Ni-Ta and Ni-W systems between 900 and 1300°C, *Mat. Sci. Eng. A.* 281 (2000) 229-233.[https://doi.org/10.1016/S0921-5093\(99\)00705-4](https://doi.org/10.1016/S0921-5093(99)00705-4)
- [57] S. Jung, T. Yamane, Y. Minamino, K. Hirao, H. Araki, S. Saji, Interdiffusion and its size effect in nickel solid solutions of Ni-Co, Ni-Cr and Ni-Ti systems, *J. Mat. Sci. Lett.* 11 (1992) 1333-1337.<https://doi.org/10.1007/BF00729354>
- [58] Y.D. Chen, The chemical composition of DZ125 superalloy(unpublished work), Beijing, 2017,
- [59] P. Caron, F. Diogolent, S. Drawin, Influence of Chemistry on the Tensile Yield Strength of Nickel-Based Single Crystal Superalloys, *Adv. Mat. Res.* 278 (2011) 345-350.<https://doi.org/10.4028/www.scientific.net/AMR.278.345>
- [60] L.Z. He, Q. Zheng, X.F. Sun, H.R. Guan, Z.Q. Hu, A.K. Tieu, C. Lu, H.T. Zhu, Effect of carbides on the creep properties of a Ni-base superalloy M963, *Mat. Sci. Eng. A.* 397 (2005) 297-304.<https://doi.org/10.1016/j.msea.2005.02.038>